Multi-omic analysis of CIC's functional networks reveals novel interaction partners and a potential role in mitotic fidelity

Yuka Takemon[1,2,*], Véronique G. LeBlanc[2,*], Jungeun Song[2], Susanna Y. Chan[2], Stephen Dongsoo Lee[2], Diane L. Trinh[2], Shiekh Tanveer Ahmad[3,4,5], William R. Brothers[2], Richard D. Corbett[2], Alessia Gagliardi[2], Annie Moradian[2], J Gregory Cairncross[4,6], Stephen Yip[7,8], Samuel A.J.R. Aparicio[7,8], Jennifer A. Chan[3,4,5], Christopher S. Hughes[7], Gregg B. Morin[2,9], Sharon M. Gorski[2,10], Suganthi Chittaranjan[2], Marco A. Marra[2,9]

[1] Genome Science and Technology Graduate Program, University of British Columbia, Vancouver, Canada
[2] Canada's Michael Smith Genome Sciences Centre, BC Cancer Research Institute, Vancouver, Canada
[3] Department of Pathology & Laboratory Medicine, University of Calgary, Calgary, Canada
[4] Arnie Charbonneau Cancer Institute, University of Calgary, Calgary, Canada
[5] Alberta Children's Hospital Research Institute, University of Calgary, Calgary, Canada
[6] Department of Clinical Neurosciences, University of Calgary, Calgary, Canada
[7] Department of Molecular Oncology, BC Cancer Research Institute, Vancouver, Canada
[8] Department of Pathology and Laboratory Medicine, University of British Columbia, Vancouver, Canada
[9] Department of Medical Genetics, University of British Columbia, Vancouver, Canada
[10] Department of Molecular Biology and Biochemistry, Simon Fraser University, Burnaby, Canada

* These authors contributed equally to this work

Simple summary

Capicua (*CIC*) is a gene that is frequently mutated in several cancer types, including stomach cancers and certain subtypes of brain tumours and sarcomas. CIC, the protein encoded by the *CIC* gene, has been shown to play a multitude of roles in both normal and cancer cell functions; however, most studies exploring these roles focus on a single aspect of CIC function and may therefore overlook complex interconnected activities in which CIC is involved. In this study, we have used multiple complementary approaches to obtain a broader view of CIC's complex functional networks. We observed novel interactions (genetic or physical) between CIC and genes/proteins involved in various aspects of cellular function, including regulation of cell division and processing of RNA molecules. Altogether, our work characterises the complexity of CIC's functional network and expands our understanding of its potential roles in cancer.

Abstract

CIC encodes a transcriptional repressor and MAPK signalling effector that is inactivated by loss-of-function mutations in several cancer types, consistent with a role as a tumour suppressor. Here, we used bioinformatic, genomic, and proteomic approaches to investigate CIC's interaction networks. We observed both previously identified and novel candidate interactions between CIC and SWI/SNF complex members, and also observed novel interactions between CIC and cell cycle regulators and RNA processing factors. We found that CIC loss is associated with an increased frequency of mitotic defects in human cell lines and an *in vivo* mouse model and with dysregulated expression of mitotic regulators. We also observed aberrant splicing in CIC-deficient cell lines predominantly at 3' and 5' untranslated regions of genes, including genes involved in MAPK signalling, DNA repair, and cell cycle regulation. Our study thus characterises the complexity of CIC's functional network and describes the effect of its loss on cell cycle regulation, mitotic integrity, and transcriptional splicing, thereby expanding our understanding of CIC's potential roles in cancers. In addition, our work exemplifies how multi-omic, network-based analyses can be used to uncover novel insights into the interconnected functions of pleiotropic genes/proteins across cellular contexts.

Keywords

CIC, genetic networks, proteomic interactions, single-cell sequencing, cell cycle, mitosis, splicing

Introduction

Capicua (CIC) is a transcriptional repressor that is impacted by somatic mutations or rearrangements in several cancer types, including undifferentiated small round cell sarcomas (~60% of cases) [1], oligodendrogliomas (~50-80%) [2,3], gastric adenocarcinomas (~9%) [4], endometrial carcinomas (~7%) [5], and melanomas (~8%) [6,7]. CIC loss has also been linked to prostate cancer [8], lung cancer [9], and T-cell lymphoblastic leukemia/lymphoma [10,11]. *CIC* alterations and/or loss of CIC activity have been associated with inferior survival outcomes in several cancer types [12–15] and with aggressive phenotypes such as increased metastatic potential [9] and resistance to kinase inhibitors [16–18]. Together, these observations are compatible with the notion that CIC functions as a tumour suppressor in several cancer types.

CIC is a transducer of receptor tyrosine kinase (RTK) signalling and functions through a default repression mechanism in which RTK activation leads to reduced CIC activity and subsequent de-repression of its target genes [19]. Targets of CIC are also themselves enriched for genes involved in the mitogen-activated protein kinase (MAPK) signalling cascade, including effectors (e.g. *PTPN9*, *SHC3/4*) and members of regulatory feedback mechanisms (e.g. *DUSP4/5/6*, *SPRY2/4*, *SPRED1/2/3*) [13,20–24]. The cancer-promoting properties observed in cells with disrupted CIC activity have been explained, at least in part, by the de-repression of one or more of its known target genes that are effectors of MAPK signalling, especially the ETS transcription factors *ETV1*, *ETV4*, and *ETV5* [8–10]. In *Drosophila*, where Cic function was originally described [25], Cic inhibits the expression of cell cycle genes (e.g. String/Cdc25, Cyclin E) and is a key mediator of Ras-driven proliferation [26,27]. Although the relationship between RAS/MAPK signalling, CIC function, and proliferation appears more complex in mammalian cells [19], loss of CIC has also been associated with proliferation in the absence of RTK signals in cancer cells and neural stem cells [16,17,22,28] and with dysregulated expression of cell cycle-related genes (e.g. *AURKA*, *CDK4*, *BUB1*) across multiple cancer types [29]. CIC has also been implicated in the development and physiology of multiple mammalian organ systems, including brain and

lung development, liver homeostasis, and T-cell differentiation [30]. It has been shown that CIC can interact with proteins such as ATXN1 [31], ATXN1L [29], and SIN3A [22,32] to mediate the expression of its targets. Interestingly, a recent study by Hwang et al. [32] demonstrated that CIC interacts with chromatin remodelers, such as several members of the Switch/Sucrose Non-Fermenting (SWI/SNF) complex—namely ARID1A, ARID1B, SMARCC1, SMARCC2, SMARCA2, and SMARCA4—to regulate neuronal differentiation. These observations give rise to the notion that CIC functions are diverse and are mediated through an increasing number of interactors only partially identified.

The increasing frequency of CIC-related publications in recent years appears to indicate a heightened level of interest in this apparently pleiotropic protein that, to date, is understood to be involved in transcriptional regulation and signal transduction to mediate phenotypes across a wide array of developmental and oncogenic contexts. Many of these CIC-related studies focus on a singular aspect of its function (e.g. transcriptional repression) in a unique context (e.g. neuronal progenitor cells). The rapid development of genomic techniques and technologies in recent years (e.g. genome-wide CRISPR screens, whole-proteome quantification, single-cell sequencing, etc.), along with access to large public datasets generated by them, have enabled powerful investigations of complex biological relationships from different angles through layering of multiple '-omic technologies (e.g. VanderSluis et al. [33], Takemon et al. [34], Shan et al. [35]). To obtain a broader view of CIC function and reveal interactions and relationships that may have remained obscured in more focused analyses, here we make use of large publicly available datasets and generate additional multi-omics data to map CIC's genetic, proteomic, and transcriptional regulatory networks in human cell lines. We identify several SWI/SNF complex members as genetic and proteomic interaction partners of CIC, reproducing previously identified protein interactions and identifying novel interactions with additional members of the complex. We also identify several cell cycle regulators in CIC's genetic and proteomic networks, and, using single-cell RNA sequencing (scRNA-seq), show that several cell cycle regulators exhibit dysregulated gene expression in CIC-deficient cell lines. Furthermore, using human cell lines and a forebrain-specific *Cic* knockout (KO)

mouse model, we demonstrate that loss of CIC is associated with an increased frequency of mitotic defects. Finally, motivated by the observation that CIC's genetic and proteomic networks include several RNA processing and splicing factors, we perform a differential splicing analysis in which we compare *CIC* wild type (WT) and KO human cell lines and find differential exon usage patterns predominantly at 3' untranslated regions (UTRs). Overall, our systematic characterisation of CIC's complex functional network reveals the effects of its loss on cell cycle regulation, mitotic integrity, and transcriptional splicing stability, thus providing new insights into CIC's potential role(s) in different biological contexts, including cancers. We argue that, in addition to revealing novel CIC functions, our study provides a blueprint for multi-omic characterisation of pleiotropic genes to uncover novel connections and functions at play across cellular and subcellular contexts.

Results

Co-essential network analysis reinforces CIC's role in MAPK signalling and identifies candidate additional functions

Genome-wide genetic perturbation screens have been used to map genetic networks, including co-essential networks and genetic interaction networks, to interrogate functional and protein complex memberships of genes [33]. Co-essential networks refer to genes that exhibit similar fitness patterns when perturbed in genetic screens, and mapping of these coordinated fitness effects (or "co-essentialities") has been used to group genes into related pathways and to identify novel gene functions in human cell lines [36,37]. Such genetic networks are much larger than protein-protein interaction networks, and can capture functional relationships that are complementary to those identified in the latter [33]. Thus, mapping of genetic networks can provide an opportunity to decipher complex interactions and functions associated with genes such as *CIC*.

Given that *CIC*'s co-essentiality network had not yet been mapped, we hypothesised that its characterisation may extend our insights into CIC function. To identify genes that exhibited co-

essentiality with *CIC* across cancer types, we leveraged fitness effect scores — a measurement of the effect of a single gene loss on cell viability [38] — that were calculated from genome-wide knockout (KO) screens performed by the Cancer Dependency Map (DepMap) project [38–40]. We calculated Pearson coefficients between fitness effect scores of *CIC* and 18,333 genes that were perturbed in 739 cancer cell lines and found 88 genes that were co-essential with *CIC* (Pearson coefficient > 0.178 and BH-adjusted *p*-value < 0.05; Figure 1a; Supplemental Table S1a; Methods). Given that two genes on the same chromosome (ie. syntenic gene pairs) may have higher rates of false positives [41], we first focused our attention on the nine co-essential genes that were non-syntenic to *CIC* (i.e. not on chromosome 19; namely *ATXN1L*, *BECN1*, *DUSP6*, *FXR1*, *KANK1*, *NFYB*, *RASA1*, *SPPL3*, and *ZCCHC12*). *ATXN1L* encodes a protein known to interact with and stabilise CIC for DNA binding [29], and *DUSP6* is a known negative regulator of MAPK signalling and target of CIC repression [21]. RASA1 is, like CIC, involved in the regulation of MAPK signalling through suppression of ERK1/2 expression [42]. Both RASA1 and NFYB are involved in the regulation of cell cycle progression and differentiation, functions with which CIC has previously been associated [30], as well as apoptosis [42–44]. *SPPL3* encodes a protease that participates in the regulation of T-cell responses by interfering with human leukocyte antigen detection [45], a function that may be related to CIC's recently described role in T-cell development [10,46–49]. *ZCCHC12* encodes a downstream effector of bone morphogenic protein signalling and has been shown to co-regulate cellular development with AP-1 and CREB [50]. As described above, CIC has been implicated in cellular development in various contexts; additionally, we and others have identified *FOS* and *FOSL1*, members of the AP-1 complex, as candidate targets of transcriptional regulation by CIC [22,24]. *BECN1* [51,52] and *KANK1* [53,54] are both involved in the regulation of apoptosis and cytoskeletal dynamics and *BECN1* is also a mediator of autophagy [51], functions with which CIC has not been associated. Finally, *FXR1* encodes an RNA-binding protein that has been implicated in the stabilisation of multiple transcripts through binding to their 5' or 3' UTRs [55–57], another role not previously associated with CIC.

To complement our efforts to identify genes with fitness effect scores similar to CIC, we next identified genes that were co-expressed with *CIC* [58]. To do this, we compared our list of co-essential genes to gene expression correlation profiles from COXPRESdb [59], as performed by Wainberg et al. [41]. The top 50 co-expressed genes (Supplemental Table S1b; Methods) included three co-essential genes: *ERF*, *BICRA*, and *PLEKHG2* (all located on chromosome 19; Figure 1a; Supplemental Table S1a). Although it is difficult to determine whether their appearance in both our co-essential screen and as top co-expressed genes is due to an artefact of their genomic proximity, the proteins encoded by these genes have been associated with functions similar to non-syntenic genes identified as co-essential with CIC, supporting the possibility that CIC does indeed share functionality with these proteins. For example, PLEKHG2 regulates the expression of CDC42, a regulator of cell cycle progression and chromosome segregation [60–62]. Notably, *ERF* perturbations had the highest correlation with *CIC*, besides *CIC* with itself, and its expression was also highly correlated with that of *CIC* (z-score = 9.6). *ERF* is located on the same chromosome band as *CIC* (chromosome 19q13.2) and is positioned directly adjacent to and transcribed in the opposite direction of *CIC*. Similar to CIC, ERF is an ETS domain transcriptional repressor and an ERK-dependent kinase that functions as an effector of the RTK signalling pathway [63,64]. Also similarly to CIC, loss of ERF has been linked to dysregulation of the cell cycle [63], developmental delays, and intellectual disability [65]. ERF and CIC were also recently shown to coordinate to regulate *ETV1* expression in prostate cancer cells [66], further supporting the notion that the two proteins function similarly and, at least in one context, cooperatively. Interestingly in the context of CIC having recently been shown to interact with the SWI/SNF complex to regulate neuronal maturation [32], the co-essential and co-expressed gene *BICRA* encodes the SWI/SNF complex member GLTSCR1 [67], further strengthening functional associations between CIC and the SWI/SNF complex. Given that several of the functions associated with CIC's co-essential genes are also known to be regulated by MAPK signalling, such as regulation of apoptotic signalling [68], cell cycle progression [69], and cell

differentiation [69], these results thus reinforce CIC's role in the regulation of RTK/MAPK signalling and highlight its potential impact on additional downstream processes that are controlled by this pathway.

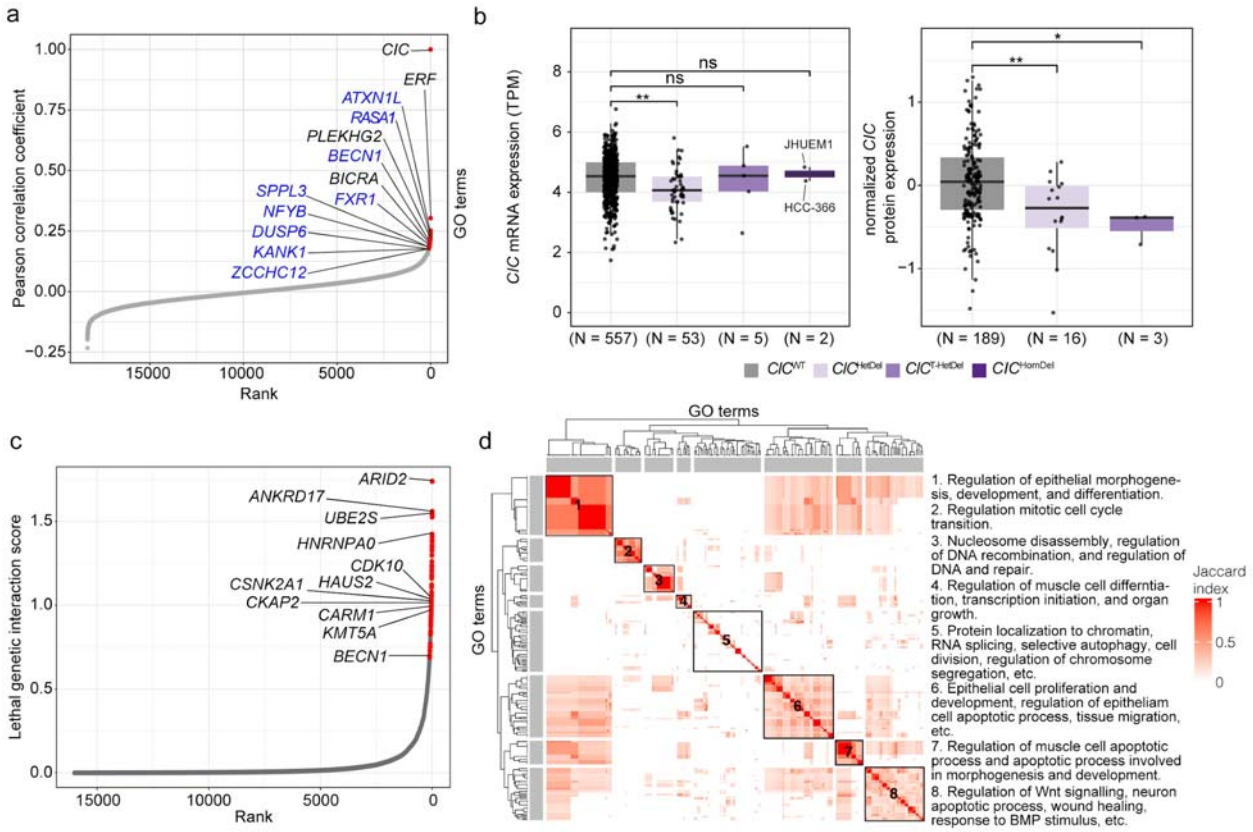

Figure 1. *CIC* is predicted to share co-essentialities and synthetic lethal interactions with regulators of cell proliferation and differentiation and chromatin remodelers.

a. Pearson correlation coefficients between the lethality probabilities of *CIC* and those of all genes targeted by DepMap genetic screens (n = 18,333) across 739 cancer cell lines. Red points indicate genes with coefficients above the inflection point (88 genes; coefficient > 0.178). Non-syntenic genes are labelled in blue and selected syntenic genes are labelled in black. **b.** Transcriptomic and proteomic data from DepMap were compared across cancer cell lines. Left: *CIC* mRNA abundance in CIC^{HomDel} (n = 2), $CIC^{\text{T-HetDel}}$ (n = 5), CIC^{HetDel} (n = 53), and CIC^{WT} (n = 557) cancer cell lines. mRNA expression values were normalised to transcripts per million (TPM). Analysis of variance (ANOVA) *p*-value = 0.00407. Right: protein expression in $CIC^{\text{T-HetDel}}$ (n = 3), CIC^{HetDel} (n = 16), and CIC^{WT} (n = 189) cancer cell lines. CIC protein expression values were normalised and mean-centred (see Methods). ANOVA (*p*-value = 0.00217) followed by Tukey's HSD analysis. **p*-value < 0.05, ** < 0.01. **c.** Ranked lethal genetic interaction scores of *CIC*. Each point represents the interaction score of a single gene KO compared between the CIC^{HomDel} (n = 2) and CIC^{WT} (n = 557) cancer cell line groups, where a higher interaction score indicates an increased likelihood of a gene KO being lethal specifically in the CIC^{HomDel} cancer cell line group (see Methods). Red points indicate significant lethal genetic interactors of *CIC* (adjusted Mann-Whitney U test p-value < 0.05 and median lethality probability > 0.5 in at least one cell line group). **d.** Heatmap showing Jaccard index similarities between 232 GO terms associated with the SL partners of *CIC* (left). The Jaccard index-based hierarchical clustering was used to summarise the GO terms into eight distinct functional groups, and these functions were summarised in the text (right).

Lethal genetic interactors of CIC are associated with regulation of apoptotic processes, cell division and differentiation, and chromatin organisation

We further leveraged DepMap data [38–40,70,71] to perform *in silico* genome-wide genetic perturbation screens to identify genes that might genetically interact with *CIC*. Specifically, we screened for genetic perturbations that, in *CIC* mutant cells, resulted in decreases or increases of cell viability relative to CIC^{WT} control cell lines (schema shown in Supplemental Figure S1a). Similar to co-essential networks, such genetic interaction networks, including synthetic lethal (SL) and alleviating genetic interactions, can reveal interactions between genes that may indicate shared functions [72–74].

Using genome sequencing data from DepMap [70], we identified a non-small cell lung cancer (NSCLC) line (HCC-366) and an endometrial carcinoma line (JHUEM1) with homozygous deleterious alterations predicted to abrogate CIC function (CIC^{HomDel}; Supplemental Table S2a-c; Methods). Notably, the mutation in JHUEM1 is exclusive to the long CIC isoform (CIC-L; Supplemental Figure S1b). This cell line may therefore retain at least some CIC activity encoded by the short CIC isoform (CIC-S). We also identified five additional cancer cell lines with deleterious and potentially *trans*-heterozygous *CIC* mutations (i.e. two or more mutations, all in regions common to the CIC-S and CIC-L isoforms; $CIC^{T\text{-}HetDel}$); 53 lines with heterozygous deleterious *CIC* mutations (six of which were exclusive to the CIC-L isoform; CIC^{HetDel}); and 557 CIC^{WT} lines (Supplemental Table S2a-c; Methods). To infer the presence of functional CIC in these different cell lines, we used DepMap transcriptome and proteome data [70,71] to analyse *CIC* mRNA and protein abundance and mRNA abundance of *ETV4* and *ETV5*, which are known targets of CIC transcriptional repression. Compared to CIC^{WT} lines, we observed a statistically significant decrease in total *CIC* mRNA levels and in *CIC*-S and *CIC*-L transcript levels only in CIC^{HetDel} lines (analysis of variance [ANOVA] followed by Tukey's Honest Significant Difference [HSD] test p-value < 0.05; Figure 1b; Supplemental Figure S1c). In contrast, we observed a significant decrease in CIC protein levels in CIC^{HetDel} and $CIC^{T\text{-}HetDel}$ lines compared to CIC^{WT} lines (ANOVA p-value = 0.0021, Tukey's

HSD test *p*-value < 0.01 and < 0.05, respectively; Figure 1b). Protein data were not available for the *CIC*^{HomDel} lines. *CIC*^{HomDel} and *CIC*$^{T\text{-}HetDel}$ cell lines both displayed trends towards higher mRNA expression of *ETV4* and *ETV5* compared to *CIC*^{WT} lines (ANOVA *p*-value > 0.05; Supplemental Figure S1d; Methods). Given the reduced CIC protein expression observed in *CIC*$^{T\text{-}HetDel}$ and *CIC*^{HetDel} lines and the moderate increases in *ETV4* and *ETV5* mRNA levels observed in *CIC*$^{T\text{-}HetDel}$ and *CIC*^{HomDel} lines, we deduced that the *CIC*^{HomDel} and *CIC*$^{T\text{-}HetDel}$ cell lines likely have reduced or perhaps lack wild type CIC activity and were therefore candidates for use in *in silico* genetic screening analyses.

We first conducted an *in silico* genome-wide screen by comparing the lethality outcomes of 18,322 gene KOs in *CIC*^{HomDel} vs *CIC*^{WT} cell lines (Supplemental Figure S1a; Methods). We used a measure called the "lethality probability", which is provided with DepMap data and which normalises the fitness effect scores to account for variability in screen quality between cell lines [38,39]. This measure is scaled from 0 to 1, where a probability of 0 indicates a non-essential gene (i.e. the gene KO did not affect cell viability) and a probability of 1 indicates an essential gene that was necessary for the survival of that cell line [38,39]. Genes that had significantly different lethality probabilities between *CIC*^{HomDel} and *CIC*^{WT} cell lines (defined as having an adjusted Mann-Whitney U test *p*-value < 0.05 and a median lethality probability > 0.5 in at least one group; Methods) were defined as candidate genetic interactors of *CIC*. We identified 70 such genes, all of which were predicted to be SL interactors of *CIC* (i.e. perturbation of these genes resulted in significantly higher lethality probabilities in *CIC*^{HomDel} lines than in *CIC*^{WT} lines; Figure 1c, Supplemental Table S3a-b). We next annotated biological functions related to the predicted SL interactors and summarised these functions into eight distinct groups (Figure 1d, Supplemental Table S3c; Methods). Functions enriched for these SL interactors included terms related to regulation of epithelial cell function (morphogenesis, differentiation, proliferation, and migration; including the genes *RREB1*, *GATA3*, *PAX8*, *CEBPB*, and *SP1*), regulation of cell cycle processes and cell division (*ANKRD17*, *CARM1*, *CSNK2A1*, *HAUS2*, *CDK10*, *BECN1*, *UBE2S*, *CKAP2*, and *KMT5A*), chromatin/nucleosome disassembly (*ARID2* and *NFE2*), histone modification and chromatin organisation (*BECN1*, *CARM1*,

GATA3, *KMT5A*, and *RIF1*) regulation of double-stranded break repair (*ARID2*, *RIF1*, and *ATP23*), RNA splicing (*LUC7L2*, *HNRNPA0*, *RBM23*), apoptotic processes (*CEBPB*, *GATA3*, *ILK*, *NKX2-5*, *PAX8*, and *PRKC1*), and Wnt signalling (*FERMT2*, *ILK*, *GATA3*, *GNAQ*, *CSNK2A1*, *NKX2-5*, and *CALCOCO1*; Figure 1d; Supplemental Table S3c). Interestingly, some of the pathways associated with *CIC*'s co-essential network, such as the regulation of apoptotic processes, cell cycle, cell division, and cell differentiation, were also associated with the predicted SL interactors of CIC. Notably, we also identified *BECN1* as being both co-essential with and a SL interactor of *CIC* (Supplemental Table S4), indicating that CIC likely plays a synergistic role either serially or in parallel with BECN1, and that the combined inactivation of these two genes, at least in the HCC-366 (NSCLC) and JHUEM1 (endometrial carcinoma) cell lines, may not be compatible with cell survival.

Our SL analysis identified *ARID2*, a SWI/SNF complex member [75], as *CIC*'s most significant SL interactor (Figure 1d, Supplemental Table S3b). This is particularly interesting given that CIC has been shown to function with the SWI/SNF complex to regulate neuronal maturation [32] and that we identified *BICRA*, which encodes another SWI/SNF member, within *CIC*'s co-essential network. Given that the SL interaction with *ARID2* was identified using an NSCLC and an endometrial carcinoma cell line and that the co-essentially network analysis was conducted using 739 pan-cancer cell lines, our data suggests that associations between *CIC* and SWI/SNF complex members, which have previously been observed in neural progenitor cells [32], may also extend to non-neural contexts.

Nuclear CIC interacts with mitotic regulators and SWI/SNF complex members

Our *in silico* analyses of *CIC*'s genetic interaction network support the notion that CIC appears to play similar roles across cellular contexts (e.g. in MAPK signal transduction, cell development, and regulation of proliferation and cell cycle). We have previously shown that CIC exerts distinct functions depending on its subcellular location (i.e. nuclear versus cytoplasmic) [76]; however, our above analyses did not provide an opportunity to discriminate between functions exerted in different subcellular

compartments. To further explore and refine CIC's functional networks in a nuclear context specifically, and given CIC's known function as a transcriptional repressor, we next set out to characterise CIC's nuclear protein interaction network, with the assumption that co-immunoprecipitation (co-IP) assays might identify interacting transcriptional regulators. We first performed co-IP assays (Methods; Figure 2a) for endogenous CIC and N-terminal MYC-fused CIC-S (using an anti-MYC antibody) in nuclear fractions purified from the HEK293A cell line (HEK-*CIC*^{WT}). The immunoprecipitates were then analysed using liquid chromatography followed by tandem mass spectrometry (MS; Methods). This yielded 291 candidate CIC-interacting proteins identified in at least two of four IP-MS replicate experiments (Supplemental Table S5), including previously identified CIC protein interactors such as ATXN2L, SMARCA2, SMARCA4, SMARCC1, SMARCC2, and SVIL [29,32]. To identify pathways and protein complexes that were overrepresented in our list of candidate interactors, we performed enrichment analyses and identified mRNA splicing, regulation of RNA metabolism, chromatin remodelling, and chromosome segregation among the significantly enriched processes (BH-adjusted *p*-value < 0.05; Supplemental Table S5; Methods). To identify candidate interactors that are common to more than one cell line, we next performed IP-MS experiments using nuclear fractions of an immortalised normal human astrocyte (NHA) cell line [77] (hereafter referred to as NHA-*CIC*^{WT}). Given CIC's known function as a transcriptional repressor, we were particularly interested in investigating whether candidate interactions with proteins involved in transcription regulation and chromatin organisation could be replicated. We therefore performed a variation of the IP-MS technique in which 'trigger peptides' [78] were used to enhance the sensitivity of the MS for a subset of these proteins of interest (Figure 2a, Supplemental Table S6; Methods). This approach revealed candidate interactions between CIC and 456 proteins in NHA cells, 156 of which we considered "high confidence" as we observed them in both the HEK and NHA lines (Supplemental Table S6; Methods). This list included the previously identified interactors ATXN2L, SMARCA2, SMARCC1, and SMARCC2. Analysis of these 156 proteins yielded significantly enriched biological processes that clustered in 26 groups of terms with similar enrichment

memberships, including groups characterised by pathways involved in RNA splicing and ribosomal and messenger RNA (rRNA and mRNA, respectively) metabolism and processing (>30 interactors, see Supplemental Table S6), DNA conformation change and duplex unwinding (including the interactors DDX3X, G3BP1, HNRNPA2B1, HP1BP3, NPM1, RUVBL1, TOP1, TTN, and XRCC5/6), chromatin remodelling and nucleosome organisation (ACTB, HNRNPC, HP1BP3, NPM1, PBRM1, RUVBL1, SMARCA2/A4/A5/C1/C2, TOP1, and TRIM28), chromatin organisation and epigenetic regulation of gene expression (ACTB, DDX21, FMR1, GLYR1, HNRNPU, MECP2, MKI67, SIN3A, SMARCA5, SNW1, TRIM28, and UPF1), telomere organisation and maintenance (DKC1, GAR1, GNL3, HNRNPA1/A2B1/C/D/U, NAT10, UPF1, XRCC5/6, and YLPM1), and intrinsic apoptotic signalling (DDX3X, DDX5, DNM1L, HNRNPK, NONO, PRKDC, RPL11, SFPQ, SNW1; BH-adjusted p-value < 0.05; Supplemental Table S6; Methods). Interestingly, among the proteins involved in mRNA metabolism and processing, we found HNRNPA0 and CDC5L. HNRNPA0 is involved in stabilising 3' UTRs of mRNA [79], and we identified the gene encoding this protein as a predicted synthetic lethal interactor of *CIC* (Supplemental Table S4). These results raise the possibility that CIC may have roles in these processes.

Consistent with our earlier observations of *CIC* interacting with members of the SWI/SNF complex (*GLTSCR1* was identified as co-essential and *ARID2* as a SL interaction partner), several members of the SWI/SNF complex were identified among the high-confidence candidate interactors of CIC, including SMARCA2, SMARCC1, SMARCC2, and PBRM1 (Supplemental Table S4). ARID1A and ARID2 were also identified as interactors in the NHA line, but not in HEK cells. Mammalian SWI/SNF has broad roles that overlap with those attributed to CIC, such as in transcriptional regulation, cell differentiation, lineage specification, DNA damage response, and RNA splicing [80,81]. Given these links and the fact that CIC and the SWI/SNF complex were recently shown to cooperatively repress the expression of neuronal development genes [32], we wanted to confirm these high-confidence interactions. To do this, we first performed reciprocal IPs by immunoprecipitating SWI/SNF complex members and

probing the IPs with western blot assays to detect CIC (Supplemental Methods). We validated the interactions between endogenous CIC and SMARCA2, SMARCC1, ARID1A, and ARID2 in the NHA-*CIC*^{WT} line (Figure 2b-e). We were unable to validate the interaction between CIC and PBRM1 (data not shown). We also performed immunofluorescence (IF) colocalization assays in *CIC*^{KO} HEK cells stably expressing a FLAG-tagged construct of the short CIC isoform (HEK-*CIC*$^{KO\text{-}D10\ +\ F\text{-}CIC\text{-}S}$) and observed a striking apparent colocalization between F-CIC-S and ARID1A, ARID2, SMARCA2, and SMARCC1 (Figure 2f-g and Supplemental Figure S2a-b). Interestingly, SMARCA2, SMARCC1, and ARID1A apparently colocalized with, and exhibited similar localization dynamics to, CIC over the entire course of the cell cycle. All four proteins were found throughout the nucleus during interphase, but appeared to be excluded from condensed chromosomes at metaphase and telophase. During early cytokinesis, colocalizing foci appeared at de-condensing chromosomes, and increasingly accumulated until completion of cytokinesis (Figure 2f-g, arrowheads). Conversely, ARID2 appeared to surround decondensing chromosomes in late telophase and colocalized with CIC only later at early cytokinesis. Although physical interactions between CIC and ARID1A and ARID2 were identified in IP-MS experiments performed in NHA cells but not detected in those performed in HEK cells, as described above, these results indicate the possibility that CIC may also interact, or at least colocalize, with these proteins in HEK cells. To further characterise these apparent colocalization patterns, we also performed proximity ligation assays (PLAs), which emit a fluorescent signal when antibodies targeting candidate protein interactors are within 40 nm of each other [82]. In HEK-*CIC*$^{KO\text{-}D10\ +\ F\text{-}CIC\text{-}S}$ cells, PLA signals were compatible with colocalization between F-CIC-S and ARID1A, SMARCA2, SMARCC1, and ARID2 during interphase (Figure 2h). Notably, the PLA signals were predominantly observed in the nucleus. Overall, these results appear to indicate spatial relationships between CIC and SWI/SNF complex proteins in both HEK and NHA cell lines, raising the possibility that CIC's functional interaction with the SWI/SNF complex extends beyond the neural progenitor context in which it was first identified [32].

To further probe the intriguing patterns of CIC nuclear localization observed above, we next performed IF assays in the NHA-*CIC*^{WT} line and a human oligodendroglioma (HOG) line (HOG-*CIC*^{WT}) [83], observing similar localization dynamics in both cell lines as were observed in the HEK cells above (Figure 2i, Supplemental Figure S2c). Ectopic expression of F-CIC-S in HEK-*CIC*$^{KO2 + F\text{-}CIC\text{-}S}$ cells also displayed similar localization dynamics as endogenous CIC (Supplemental Figure S2d). To determine if CIC's distinct dynamic localization pattern was potentially mediated by mitotic structures, we performed IF colocalization assays using markers of □-tubulin, CENPA, and AURKB to observe spindles, centromeres, and the midbody, respectively (Supplemental Figure S2e-g). CIC did not appear to be associated with spindle structures, centromeres or kinetochore attachments, or the midbody over the course of the cell cycle.

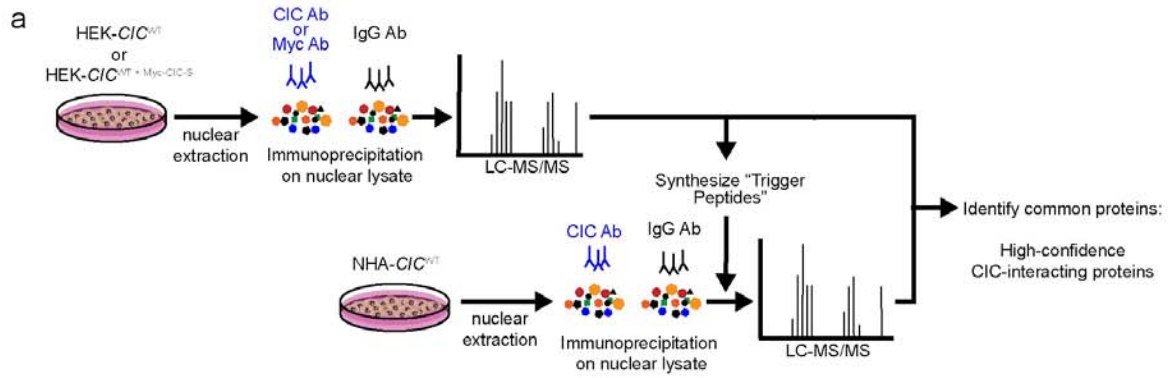
a
HEK-CIC^WT
or
HEK-CIC^WT + Myc-CIC-S
nuclear extraction
CIC Ab or Myc Ab
IgG Ab
Immunoprecipitation on nuclear lysate
LC-MS/MS
Synthesize "Trigger Peptides"
NHA-CIC^WT
CIC Ab
IgG Ab
nuclear extraction
Immunoprecipitation on nuclear lysate
LC-MS/MS
Identify common proteins:
High-confidence CIC-interacting proteins

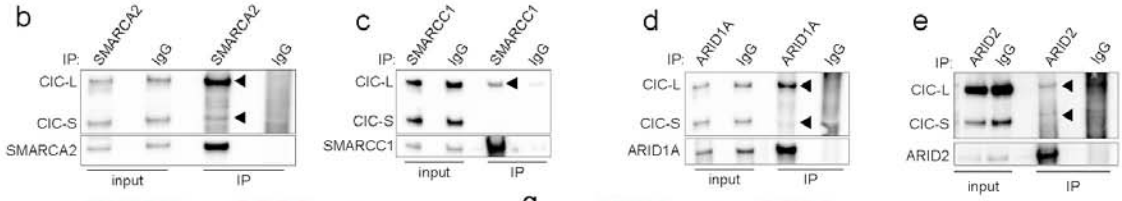
b
IP: SMARCA2 IgG SMARCA2 IgG
CIC-L
CIC-S
SMARCA2
input IP
c
IP: SMARCC1 IgG SMARCC1 IgG
CIC-L
CIC-S
SMARCC1
input IP
d
IP: ARID1A IgG ARID1A IgG
CIC-L
CIC-S
ARID1A
input IP
e
IP: ARID2 IgG ARID2 IgG
CIC-L
CIC-S
ARID2
input IP

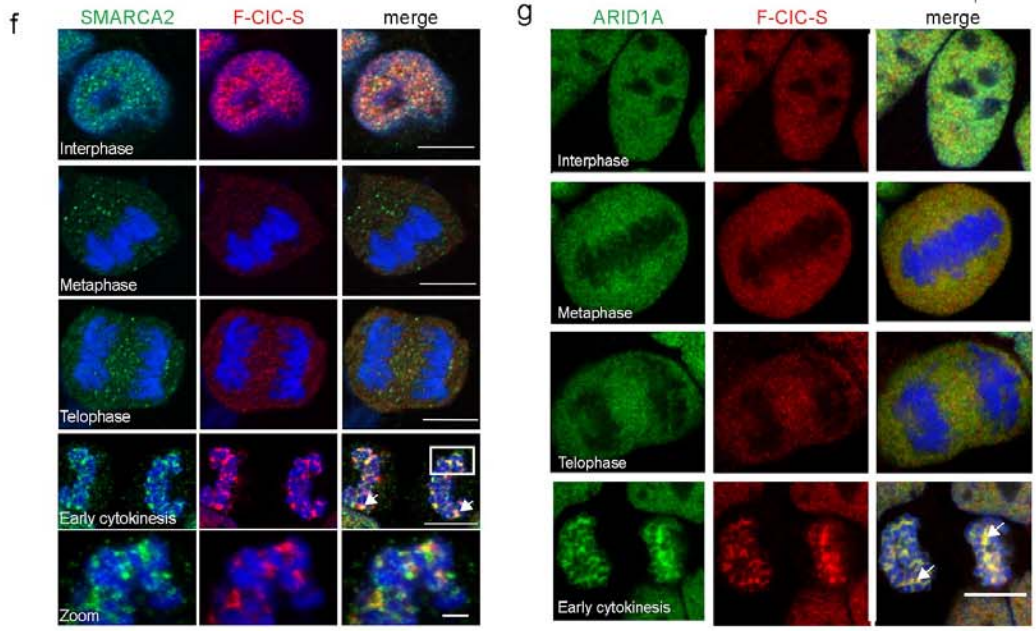
f
SMARCA2
F-CIC-S
merge
Interphase
Metaphase
Telophase
Early cytokinesis
Zoom
g
ARID1A
F-CIC-S
merge
Interphase
Metaphase
Telophase
Early cytokinesis

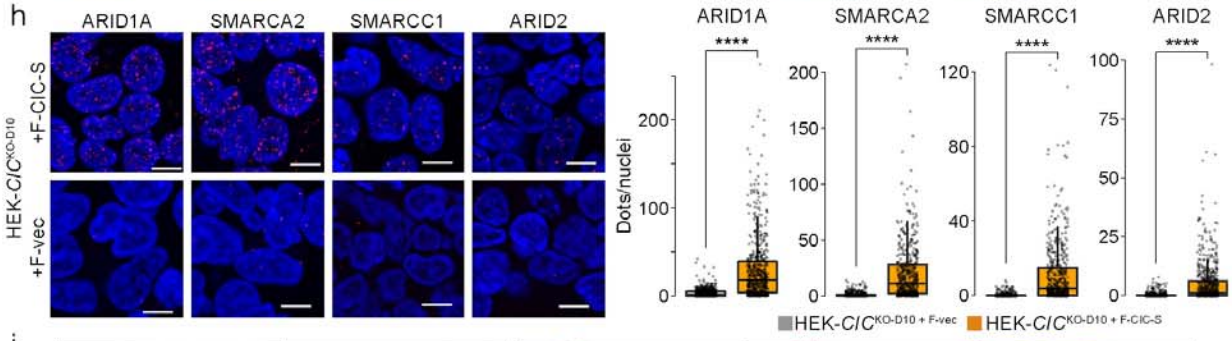
h
ARID1A
SMARCA2
SMARCC1
ARID2
HEK-CIC^KO-D10
+F-CIC-S
+F-vec
Dots/nuclei
****
HEK-CIC^KO-D10 + F-vec
HEK-CIC^KO-D10 + F-CIC-S

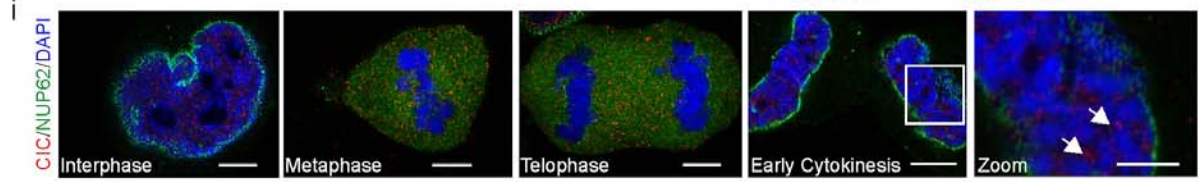
i
CIC/NUP62/DAPI
Interphase
Metaphase
Telophase
Early Cytokinesis
Zoom

Figure 2. CIC interacts with members of the SWI/SNF complex.
a. Workflow of CIC IP-MS in HEK-*CIC*^{WT} and NHA-*CIC*^{WT} cell lines. See Methods section for more detail. **b**-**e**. Reciprocal IPs confirming interactions between CIC and select SWI/SNF subunits. SMARCA2 (b), SMARCC1 (c), ARID1A (d), and ARID2 (e) were immunoprecipitated from nuclear lysates of the parental NHA-*CIC*^{WT} cell line, and CIC interaction was visualised using western blotting. Input lanes indicate nuclear lysate samples used as input for the respective IPs. CIC-L and CIC-S bands are marked with arrowheads. **f-g**. Localization of F-CIC-S (FLAG, red), SMARCA2 (f, green), and ARID1A (g, green) in HEK-*CIC*$^{KO\text{-}D10\ +\ F\text{-}CIC\text{-}S}$ cells at phases of the cell cycle, visualised using IF. DNA was stained with DAPI (blue). Arrows indicate colocalization of CIC and the relevant interactor at early cytokinesis (yellow foci). Scale bars: 10 µm and 5 µm (zoomed image in f). **h**. Left: representative PLAs using antibodies against FLAG and ARID1A, SMARCA2, SMARCC1, or ARID2 in HEK-*CIC*$^{KO\text{-}D10}$ cells expressing F-CIC-S (HEK-*CIC*$^{KO\text{-}D10\ +\ F\text{-}CIC\text{-}S}$, top) or an empty vector (HEK-*CIC*$^{KO\text{-}D10\ +\ F\text{-}Vec}$, bottom). DNA was visualised using DAPI staining (blue). PLA signals indicating proximity of the proteins assayed (< 40 nm) are red spots. Right: Tukey boxplots showing quantifications of PLA spots per nuclear region. ARID1A, n = 732 and 583; SMARCA2, n = 564 and 533; SMARCC1, n = 564 and 533; ARID2, n = 564 and 588 (nuclei counts for HEK-*CIC*$^{KO\text{-}D10\ +\ F\text{-}Vec}$ and HEK-*CIC*$^{KO\text{-}D10\ +\ F\text{-}CIC\text{-}S}$, respectively). ****$p$-value < 0.0001 (Welch's t-test). **i**. IF staining of endogenous CIC (red) and the nuclear envelope protein NUP62 (green) in the parental NHA-*CIC*^{WT} line. CIC shows a punctate localization pattern (arrows) throughout the decondensing nucleus. Scale bars: 10 µm and 5 µm (zoomed image).

Loss of CIC is associated with mitotic defects in mammalian cells

While performing the IF assays described above, we observed that the *CIC*^{KO} cells appeared to display a higher frequency of defective mitosis (e.g. improper metaphase alignment, lagging chromosomes) compared to *CIC*^{WT} cells. To investigate this further, additional IF assays in the NHA lines were used to confirm that NHA-*CIC*^{KO} lines had an increased frequency of mitotic defects compared to the parental NHA-*CIC*^{WT} cells (Figure 3a-b). Specifically, the *CIC*^{KO} lines (NHA-*CIC*$^{KO\text{-}A2}$ and NHA-*CIC*$^{KO\text{-}H9}$) showed 2.2 - 2.5-fold increases in metaphase alignment defects (two-sided Student's t-test p-value < 0.05) and 2 - 2.3-fold increases in chromosome segregation defects (e.g. lagging chromosomes and micronuclei) at telophase/cytokinesis (p-value < 0.01). We also observed a significant increase in metaphase defects in HEK-*CIC*^{KO} cell lines compared to HEK-*CIC*^{WT} cell lines (Supplemental Figure S3), indicating that the association between CIC loss and increased frequency of mitotic defects is not specific to the NHA-derived lines.

To determine if this phenotype extended beyond mammalian cell lines, we performed additional IF assays in brain sections from E13.5 mice with forebrain-specific *Cic* loss (*Cic*$^{fl/fl}$; *FoxG1*$^{cre/+}$) and from

heterozygous control mice (*Cic*$^{fl/+}$; *FoxG1*$^{cre/+}$) [84]. Consistent with our *in vitro* results, *Cic*-null cells in the mitotically active ventricular zone displayed an increased frequency of mitotic defects, including lagging chromosomes and micronuclei (average 2.5-fold increase, two-sided Student's *t*-test *p*-value < 0.0001; Figure 3c). Together, these observations support a previously unappreciated relationship between CIC loss and mitotic defects in mammalian cells *in vitro* and *in vivo*.

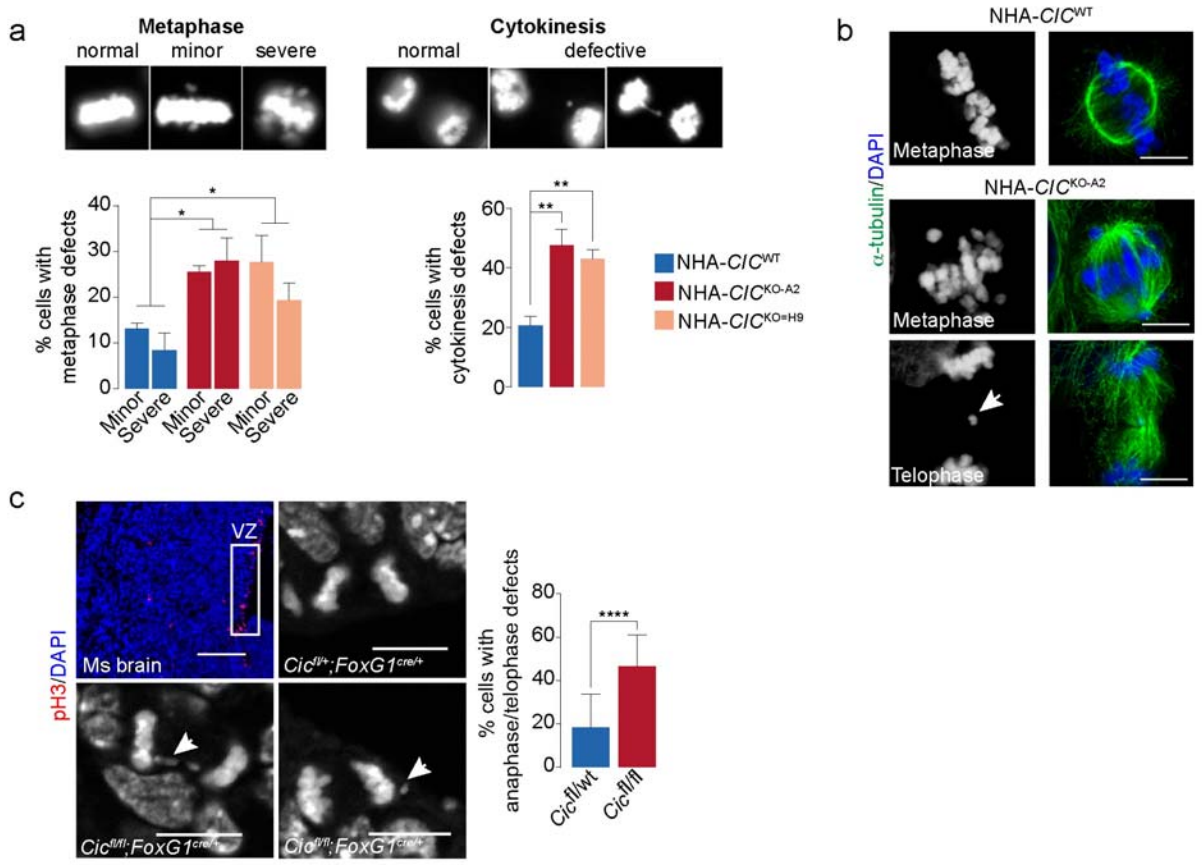

Figure 3: Cells lacking CIC have an increased frequency of mitotic defects.
a. Top: representative images of NHA cells with normal or defective metaphase and cytokinesis. Bottom: proportions of cells from indicated cell lines assigned to each category. Bars represent the mean from three independent experiments and error bars indicate s.e.m. NHA-*CIC*^{WT}, n = 146 and 122; NHA-*CIC*$^{KO-A2}$, n = 99 and 94; NHA-*CIC*$^{KO-H9}$, n = 104 and 89 (metaphase and cytokinesis cell counts, respectively). **b**. Representative images of an NHA-*CIC*^{WT} cell with normal metaphase (top) and NHA-*CIC*$^{KO-A2}$ cells with defective metaphase alignment (middle) and a lagging chromosome at telophase (arrowhead, bottom). Left: DAPI staining alone. Scale bars: 10 µm. **c**. Left: mitotically active (boxed) ventricular zone (VZ) region from an E13.5 Cic$^{fl/+}$;FoxG1$^{cre/+}$ mouse forebrain and representative images of a normal cell division in a *Cic*$^{fl/+}$;*FoxG1*$^{cre/+}$ mouse (top right) and a lagging chromosome and a micronucleus in

Cic$^{fl/fl}$;*FoxG1*$^{cre/+}$ mice (arrowheads, bottom left and right, respectively). Right: proportions of cells with defective anaphase/telophase. Bars represent the mean from four animals for each genotype and error bars indicate s.e.m (n = 186 cells for *Cic*$^{fl/+}$;*FoxG1*$^{cre/+}$ mice and 180 for *Cic*$^{fl/fl}$;*FoxG1*$^{cre/+}$ mice). Scale bars: 100 µm (top left) and 10 µm. *p-value < 0.05, ** < 0.01, **** < 0.0001 (two-sided Student's t-test [a,c]).

Loss of CIC is associated with transcriptional dysregulation across all cell cycle phases

Given CIC's dynamic pattern of nuclear localization and the association between its loss and increased mitotic defects, we hypothesised that CIC's effects on gene expression regulation may depend on the cell cycle. Since dysregulated expression of dynamically expressed genes may not be detectable in asynchronous bulk cell populations, and synchronisation through either chemical or physical means can introduce confounding artefacts [85,86], we therefore performed single-cell RNA-seq (scRNA-seq) on asynchronous *CIC* wild type (parental NHA line, NHA-*CIC*^{WT}) and *CIC*^{KO} (NHA-*CIC*$^{KO-A2}$ and NHA-*CIC*$^{KO-H9}$ lines) cells. To characterise the transcriptional profiles of CIC-proficient and CIC-deficient cells at different phases of the cell cycle, we first scored cells for defined cell cycle phases (G2, G2/M, M/G1, G2/S, and S phases) [87] using approaches described previously [88,89] (Methods). For each phase, we then performed a differential expression analysis comparing *CIC*^{WT} and *CIC*^{KO} cells assigned to that phase (Figure 4a and Supplemental Table S7) and, to explore coordinated patterns in gene expression differences, we also performed a gene set enrichment analysis specific to each phase (Supplemental Table S8). The canonical CIC targets *ETV1/4/5* were among the genes found to be significantly more abundantly expressed in *CIC*^{KO} cells at each phase (*ETV4*) or some phases (G1/S for *ETV1*, G1/S and M/G1 for *ETV5*; BH-adjusted p-value < 0.05 and absolute fold-change > 1.5), supporting the validity of our approach. Genes overexpressed in *CIC*^{KO} cells were also consistently found to be enriched for targets of RAS/MAPK signalling (e.g. *ENG*, *ETV1/4/5*, *GNG11*, *GYPC*, *SOX9*) as has previously been shown using bulk transcriptome profiling of CIC-deficient cell lines and tumours [13,20–22], indicating that CIC plays a role in the regulation of this signalling cascade at all stages of the cell cycle. In line with CIC's known role as a transcriptional repressor that interacts with chromatin modifiers such as histone deacetylases and the SWI/SNF complex [22,32], we also observed enrichment of chromatin-related terms

within overexpressed genes. Given that our IP-MS analysis identified MECP2 as a high-confidence physical interactor of CIC, of particular interest was the Reactome term "transcriptional regulation by MECP2" (M27862), which was enriched or trended towards enrichment across all five phases (Figure 4b). Genes belonging to this term and that were found to be differentially expressed in *CIC*^{KO} cells in at least one phase included *HIPK2*, which encodes a serine-threonine kinase that regulates the activity of a wide range of transcription factors and chromatin regulators [90], and *TNRC6B* and *DGCR8*, both of which are involved in RNA processing [91–93]. Other transcriptional activators, such as *ATF4*, *CREB3L2*, *FOSL1*, *MLXIP*, *RXRA*, *SMAD3*, *SOX9/12*, *SREBF1/2*, and *STAT6* were also found to be more highly abundant in *CIC*^{KO} cells, especially at the G1/S and S phases. Conversely, genes encoding proteins involved in transcriptional repression were also identified among those overexpressed in *CIC*^{KO} cells, including e.g. the polycomb repressive complex 1 (PRC1)-related genes *CBX6* and *PHC2*, the nucleosome remodelling and deacetylase (NuRD) complex members *CHD3*, *MBD3*, and *GATAD2A*, and the histone deacetylase *HDAC7*.

Although elevated expression of target genes in *CIC*^{KO} cells could be a direct consequence of CIC loss given its function as a transcriptional repressor, across all cell cycle phases approximately half (mean 51%, range 45-60%) of all significantly differentially expressed genes displayed lower expression in *CIC*^{KO} cells (Figure 4a). This is in agreement with results we and others have shown previously from bulk RNA-seq profiling of CIC-proficient and -deficient cell lines and tumour samples [21,29,94]. Interestingly, several gene sets related to cell cycle regulation and checkpoints were enriched for downregulated genes, driven by genes such as *CCNB1* (significantly less abundant in S and G2/M *CIC*^{KO} cells), *CDK1* (G1/S), *MAD2L1* (S and G2/M), *CENPK* (M/G1), and *CCNE2* (G1/S; Figure 4c). *YWHAQ* and *YWHAB*, which are members of the 14-3-3 family of proteins that bind to CIC and inhibit its activity [95] and which also play a role in cell cycle checkpoints and regulation of apoptosis [96], were also found to be underexpressed in *CIC*^{KO} cells (*YWHAQ* reaching statistical significance in all phases except G2/M and *YWHAB* reaching statistical significance in S-phase cells only). Echoing results of our IP-MS

analysis, we also observed an enrichment of genes involved in RNA processing and splicing among genes with lower expression in *CIC*^{KO} cells. These include the small nuclear ribonucleoprotein core protein family members *SNRPB2* and *SNRPD2*, the heterogeneous nuclear ribonucleoproteins *HNRNPH3* and *HNRNPA2B1*, the splicing factor 3B subunit *SF3B4*, and the spliceosome component *PRPF31*, all of which were significantly under-expressed in G1/S-phase *CIC*^{KO} cells. Interestingly, our results also indicated that *NPM1* had significantly lower expression in G2/M-phase *CIC*^{KO} cells, although it showed a similar trend at all phases, especially in the *CIC*$^{KO\text{-}A2}$ cell line (Fig 4c). *NPM1* is frequently mutated in acute myeloid leukaemia and encodes a protein involved in functions related to many of the ones mentioned above, including centrosome licensing (and thereby genome stability), ribosome biogenesis, the p53-mediated stress response, and inhibition of cell growth and proliferation [97]. Notably, we also identified NPM1 as a high-confidence physical interactor of CIC (Supplemental Table S4).

To investigate whether genes that were differentially expressed in *CIC*^{KO} cells might be directly regulated by CIC, we compared our gene list with a set of 150 high-confidence CIC binding sites that our group previously identified in the NHA-*CIC*^{WT} line using chromatin immunoprecipitation followed by sequencing (ChIP-seq) [24]. Of the 135 genes associated with these binding sites (Supplemental Table S9), transcripts for 10 of them — *DUSP4*, *DUSP5*, *ETV4*, *ETV5*, *FOSL1*, *HMGA1*, *MAFF*, *OSGIN1*, *TBC1D14*, and *TBC1D22A* — were differentially abundant between NHA-*CIC*^{WT} and NHA-*CIC*^{KO} cells in at least one cell cycle phase in our scRNA-seq data (Supplemental Table S4). All of these genes were more highly expressed in NHA-*CIC*^{KO} cells, which is consistent with CIC's known function as a transcriptional repressor. Indeed, *ETV4* and *ETV5* are well-established targets of CIC transcriptional regulation [19], and *DUSP4* [21,22,32], *DUSP5* [22], *FOSL1* [22], and *MAFF* [32] have also previously been proposed direct targets of CIC in different cellular contexts. FOSL1 is a proto-oncogene and a member of the FOS gene family, which encodes a group of proteins that can dimerize with proteins of the JUN family to form the transcription factor AP-1. FOSL1 is activated by the RAS/MAPK signalling cascade through phosphorylation by ERK2, ERK5, and RSK2 [98]; however, these results indicate the

possibility that *FOSL1* expression could be further regulated by CIC activity downstream of MAPK signalling. MAFF, similarly to FOSL1, is a member of the basic leucine zipper (bZIP) family of transcription factors and can also participate in the formation and binding activity of the AP-1 complex [99]. It has been associated with a variety of functions, mostly related to the stress response, and its activity has been implicated in cancer [100,101]. Interestingly, MAFF has also been implicated as a feedback regulator of the MAPK signalling cascade, potentially downstream of AP-1 activity [102]. Notably, DUSP4 and DUSP5 are also important feedback regulators of MAPK signalling [103], similarly to other genes that have previously been shown to be targets of CIC transcriptional regulation (e.g. *DUSP6*, *SPRY2/4*, *SPRED1/2*). OSGIN1 is an oxidative stress and DNA damage response tumour suppressor that acts downstream of and in concert with p53 to induce mitochondrial cytochrome c release and apoptosis [104]. Overall, these results indicate that CIC appears to regulate the expression of genes involved in a wide range of functions, including MAPK signalling, transcriptional regulation, mitotic checkpoint activity, and RNA processing. Notably, our results also indicate that CIC regulates the expression of similar groups of genes across different phases of the cell cycle. Furthermore, candidate direct targets of CIC transcriptional regulation appear enriched for genes involved in functions that we have repeatedly identified in this study, including MAPK signalling, AP-1 activity, and apoptosis, further implicating CIC activity within these functional groups.

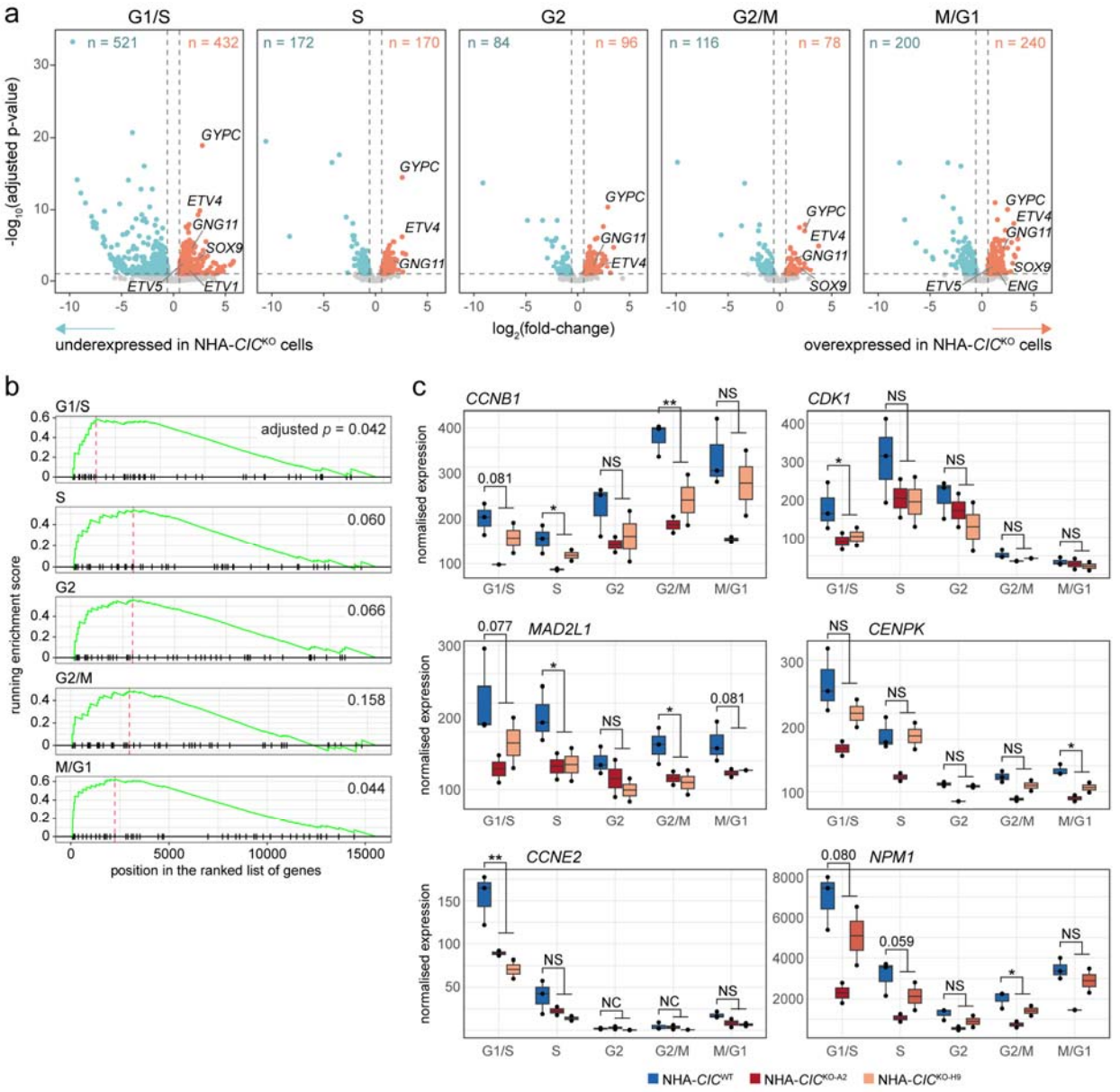

Figure 4: *CIC*^{KO} cells display dysregulated expression of genes involved in chromatin organisation and cell cycle checkpoints

a. Volcano plots depicting differential expression analysis results for *CIC*^{KO} versus *CIC*^{WT} cells assigned to each indicated phase. Genes considered to be significantly differentially expressed (BH-adjusted p-value < 0.05 and absolute fold-change > 1.5) are coloured and their numbers are indicated at the top of each plot. **b**. Graphical representation of GSEA results for the Reactome term "transcriptional regulation by MECP2". **c.** Normalised expression of indicated genes across cell lines and phases. *BH-adjusted *p*-value < 0.05, ** < 0.01 (Wald test as implemented by DESeq2), NS: non-significant, NC: adjusted *p*-value not calculated due to low expression (see Methods).

CIC binding sites overlap with a subset of SWI/SNF binding sites

In light of our observations of genetic and physical interactions between CIC and members of the SWI/SNF complex, and of a recent study showing that CIC functions with the SWI/SNF complex to regulate gene expression in the context of neuronal development [32], we set out to explore whether CIC may function cooperatively with the SWI/SNF complex to regulate gene expression in contexts beyond the one investigated by Hwang et al. [32]. To do this, we obtained publicly available ChIP-seq data for CIC [22] and ARID1A, BRD4, BRD9, and SMARCA4 [105] generated from mouse embryonic stem cell (mESC) cultures. We chose these datasets to limit, as much as possible, biological variability between cell lines, since we were unable to find SWI/SNF ChIP-seq data from human cell lines in which CIC ChIP-seq has been performed. Supporting the translatability of human and mouse datasets, 25 orthologous gene pairs were associated with CIC peaks in both the NHA dataset [24] and the mESC dataset [22] (Supplemental Table S10), including the established CIC targets *CCND1/Ccnd1*, *DUSP4/Dusp4*, *ETV4/Etv4*, *ETV5/Etv5*, *GPR3/Gpr3*, *LRP8/Lrp8*, *PTPN9/Ptpn9*, *SPRED2/Spred2*, and *SPRY4/Spry4*. Of the 108 peaks identified in the mESC CIC ChIP-seq dataset (see Methods), 26 overlapped with ARID1A peaks (hypergeometric test $p = 1.38\text{x}10^{-12}$), 60 with BRD9 peaks ($p = 1.71\text{x}10^{-40}$), 84 with BRD4 peaks ($p = 2.26\text{x}10^{-38}$), and 102 with SMARCA4 peaks ($p = 8.66\text{x}10^{-32}$). Notably, of the 100 genes associated with these 108 mESC CIC peaks, the human orthologues for 10 of them were found to be differentially expressed in at least one cell cycle phase in our scRNA-seq data (*DDX54*, *DUSP4*, *DUSP5*, *ETV1*, *ETV4*, *ETV5*, *HSPG2*, *MAFF*, *SREBF2*, and *TTLL12*). The 14 peaks associated with these 10 genes all overlapped with peaks from at least one of the three SWI/SNF members (14/14, 13/14, 10/10, and 4/14 sites overlapped with SMARCA4, BRD4, BRD9, and ARID1A peaks, respectively; Supplemental Table S10). Together, these results indicate the possibility that CIC may indeed function with the SWI/SNF complex to regulate transcription.

CIC loss destabilises splicing at untranslated regions

Given our observations that RNA splicing factors share genetic and proteomic interaction with CIC and that RNA splicing genes are dysregulated in CIC-deficient cell lines, we posited that loss of CIC may have a global effect on transcript splicing. To investigate this, we applied Whippet, a tool for *de novo* detection and quantification of alternative splicing events using Shannon entropy-based methods [106], to bulk RNA-seq data we generated previously from three biological replicates of each of the NHA-*CIC*^{WT}, NHA-*CIC*$^{KO-A2}$, and NHA-*CIC*$^{KO-H9}$ lines ([24]; GEO accession: GSM5708721). We detected 29,020, 28,104, and 27,042 alternative splicing events in at least two replicates of the NHA-*CIC*^{WT}, NHA-*CIC*$^{KO-A2}$, and NHA-*CIC*$^{KO-H9}$ cell lines, respectively (Supplemental Table S11a). Whippet attributes entropy scores to genes identified as undergoing alternative splicing, with scores ranging from 0 to $\log_2$(number of isoforms). We did not observe differences in the overall distribution of entropy scores between the NHA-*CIC*^{WT} line and either the NHA-*CIC*$^{KO-A2}$ or NHA-*CIC*$^{KO-H9}$ lines (Kolmogorov–Smirnov test p-value > 0.05 in both comparisons; Figure 5a), nor did we observe a significant difference in the proportion of high-entropy events (entropy scores > 1.5; i.e. more than three expressed isoforms) between the NHA-*CIC*^{WT} and NHA-*CIC*^{KO} cell lines (Supplemental Figure S4a). Notably, however, the proportion of high-entropy events identified in the NHA cell lines (~2%; Supplemental Figure S4a) was higher than those observed for hepatocellular carcinoma samples, which showed ~0.10% and ~0.12% high-entropy events in control and tumour samples, respectively [106]. This is consistent with previous reports showing that brain cells have higher isoform complexity than other tissue types [107]. Together, these results indicate that CIC loss does not appear to result in marked global changes in alternative splicing events, at least in NHA cells.

To determine whether CIC loss affected specific types of splicing events, we used Whippet to perform differential usage analysis and categorised the events by splicing type, comparing the parental NHA-*CIC*^{WT} line to both NHA-*CIC*^{KO} lines. We identified 787 significant differential splicing events affecting 468 genes (absolute Delta Ψ > 0.1 and probability > 0.9, as described by Georgakopoulos-

Soares et al. [108]; Figure 5b; Supplemental Table 11b). Interestingly, of the eight different types of splicing events that Whippet can detect—namely alternative acceptor, alternative donor, alternative first exon, alternative last exon, core exon, retained intron, tandem transcription end sites, and tandem transcription start sites (TSSs) [106]—the splicing events that were found to be differential between *CIC*^{WT} and *CIC*^{KO} cells were all categorised as one of only three types: transcriptional end sites (or tandem polyadenylated [poly-A] sites; 589 events affecting 360 genes), TSSs (or tandem 5'UTR; 195 events affecting 109 genes), and retained introns (three events affecting three genes; Figure 5b; Supplemental Figure 4b; Supplemental Table 11b). Furthermore, we observed more genes containing events that led to a shorter 3' UTR (i.e. usage of an earlier poly-A site, ~200 genes) compared to those that lengthened it (~150 genes) in the NHA-*CIC*^{KO} cell lines (Figure 5c). Conversely, tandem TSS events were equally distributed between those that lengthened or shortened the 5' UTR. These results may indicate that loss of CIC can affect 3' end usage and, to a lesser extent, 5' end usage, and that it may favour the shortening of 3' UTRs. To investigate the genes affected by differential splicing events upon CIC loss, we annotated these genes and summarised their functions into 18 categories (Supplemental Table S11c; Supplemental Figure 4c). We found genes associated with roles such as regulation of vesicle transport, apoptosis and autophagy, cell development and differentiation, microtubule cytoskeleton, cell cycle, DNA repair, and chromosome segregation (Supplemental Table S11c). Interestingly, the SWI/SNF complex members *ARID1A* and *ARID1B* both displayed alternative TSS usage in the *CIC*^{KO} cells (Supplemental Table S11b). The differential intron retention events affected the ribosomal proteins *RPL7A* and *RPL35A* (exclusion in the *CIC*^{KO} cells; Figure 5d-e) and the ubiquitin conjugate enzyme *UBE2N* (inclusion; Figure 5f), which is involved in DNA repair [109]. Differential 3'UTR usage was detected in *BCL2L11*, which encodes the proapoptotic BH3-only protein BIM, resulting in a shortening of this region in CIC^{KO} cells. Interestingly in rat neurons, ERK signalling was shown to regulate *Bim* expression via the 3'UTR [110]. Given that 3'UTR length can affect the stability, localization, and

translation of mRNA [111], these results suggest that loss of CIC may affect the functions of these processes through dysregulation of transcript splicing.

Given that UTR length and intron retention events have both been shown to affect gene expression [112–114], we next compared the list of genes affected by significant alternative splicing events to those that were found to be differentially expressed in our scRNA-seq data. We identified 51 genes affected by alternative splicing that were also significantly differentially expressed (31 and 20 genes upregulated and downregulated in NHA-*CIC*^{KO} cells, respectively; Supplemental Table S11d). Consistent with the notion that intron retention can downregulate gene expression [114], *RPL7A*, which was found to exclude an intron in the NHA-*CIC*^{KO} cell lines that was retained in the NHA-*CIC*^{WT} line (Figure 5d), showed higher expression in NHA-*CIC*^{KO} lines at G1/S, S, and M/G1 phases (Supplemental Figure S4d), whereas *UBE2N*, which retained an intron in *CIC*^{KO} cells (Figure 5f) was significantly downregulated in G1/S-phase *CIC*^{KO} cells (Supplemental Figure S4d). We also observed several genes associated with cell cycle regulation, namely *CCNC* [115], *HMGA2* [116], and *PLAC9* [117], that had differential UTR events as well as differential gene expression (Figure 5i-k and Supplemental Figure S4d). Interestingly, *NRG1*, which encodes the NRG1 ligand that binds to ERBB receptors to activate MAPK and other signalling pathways [118] and which is also involved in neuronal development [119], was also found to include an additional TSS in *CIC*^{KO} cells (Figure 5l) and was overexpressed in G1/S-phase *CIC*^{KO} cells (Supplemental Figure S4d). *NRG1* gives rise to >30 isoforms, which are grouped into six types (I-VI) [120]. The alternative TSS identified in *CIC*^{KO} cells affects NRG1 isoforms 3, 6, 7, and 8 (Uniprot ID Q02297-3, Q02297-6, Q02297-7, and Q02297-8, respectively), which share a common TSS and which belong to types II (isoform 3, predominantly expressed in mesenchymal cells) and III (isoforms 6-8, the major isoforms expressed in neurons) [119]. Since type III NRG1 isoforms bind ERBB2, ERBB3, and ERBB4 [118,120], [118,120] Altogether, our profile of the alternative splicing patterns in NHA cell lines shows that loss of CIC is associated with destabilised splicing predominantly at UTRs. A subset of genes affected by alternative splicing also show dysregulated gene expression, including genes associated with

roles that were previously known or have emerged as part of this study as being associated with CIC, such as MAPK signalling, DNA repair, cell cycle regulation, and neuronal development.

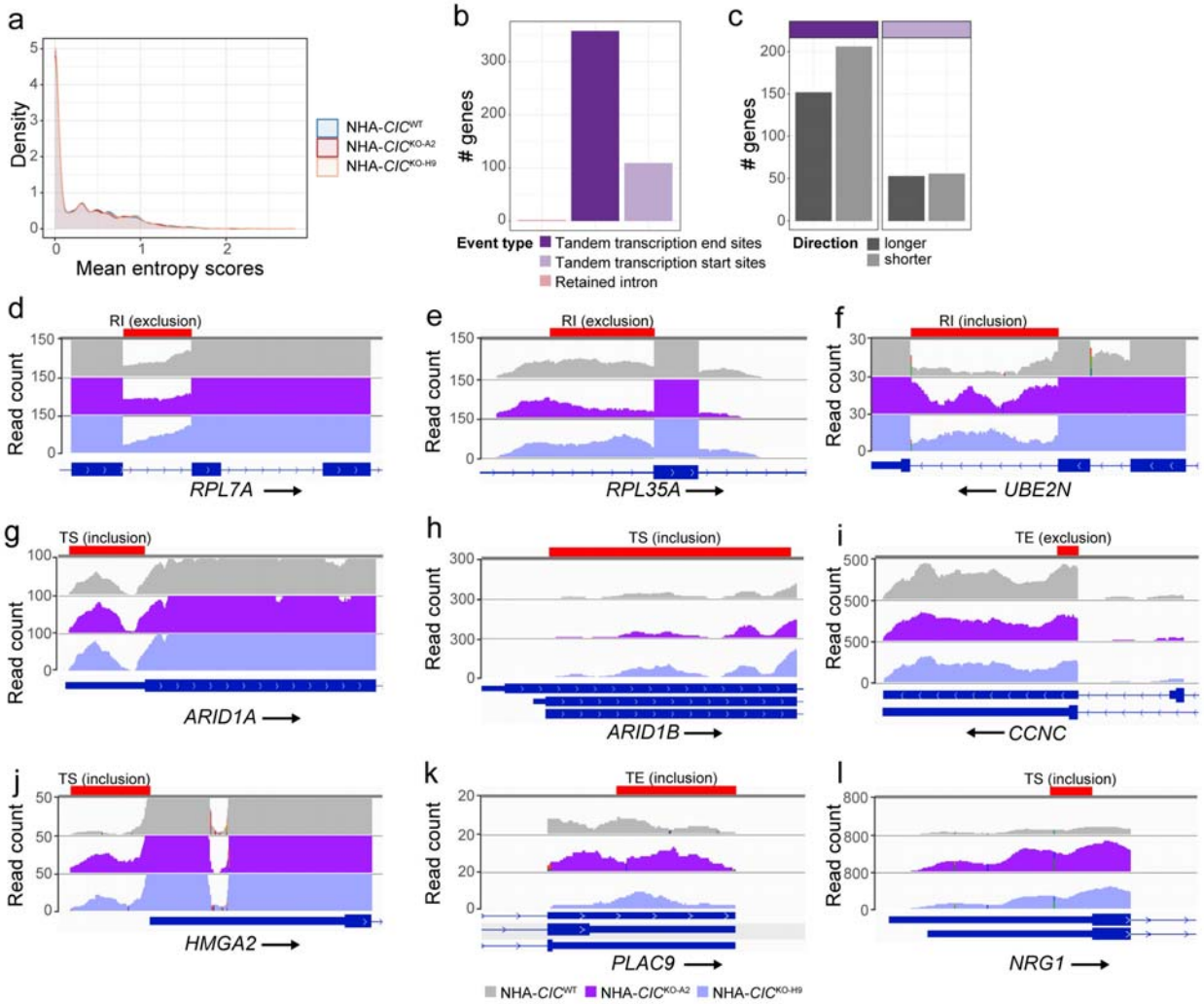

Figure 5: *CIC*^{KO} cells show differential splicing predominantly at UTRs.
a. Density plot showing the proportion of genes across entropy scores in NHA cell lines. Entropy scores are shown as the mean of three replicates. Kolmogorov–Smirnov tests between the distributions of the NHA-*CIC*^{WT} line and both NHA-*CIC*^{KO} lines were not significant (p-value > 0.05). **b**. The number of genes affected by significant differential splicing events (absolute Delta Ψ > 0.1 and probability > 0.9) that were detected when comparing the NHA-*CIC*^{WT} line to both NHA-*CIC*^{KO} lines combined, grouped into indicated categories (see Supplemental Figure S4b for all detected events). **c**. The number of genes with alternative transcriptional start or end site events from panel b that led to either longer or shorter UTR sites. See panel b for event type colour legend. **d-l**. Representative images from IGV of one replicate each of the NHA-*CIC*^{WT}, NHA-*CIC*$^{KO-A2}$, and NHA-*CIC*$^{KO-H9}$ lines showing genes affected by significant differential splicing events. Red bars highlight the genomic regions where the events were detected, and the event types are indicated above (retained intron [RI], tandem transcription end site [TE], and tandem

transcription start site [TS]). RefSeq transcript models are shown in dark blue below the sample tracks, with transcriptional direction indicated by arrows.

Discussion

In this study, we used bioinformatics, mass spectrometry, single-cell RNA-seq, and microscopy techniques to expand our understanding of CIC function in human and mouse cells and tissues. Results from these orthogonal approaches converged to implicate CIC in cell cycle regulation and splicing in addition to its known function as an effector of MAPK signalling (see Supplemental Table S4 for a summary of genes/proteins that were identified as part of CIC's functional networks using different 'omics approaches). Furthermore, we uncovered multiple lines of evidence indicating that CIC interacts with the SWI/SNF complex in additional cellular contexts than the neuronal progenitor one where the interaction was first observed [32], and that CIC may rely on this interaction for some of its functions in these novel cellular contexts. Strikingly, we also observed that CIC loss was associated with an increased frequency in mitotic defects in human cell lines and in an *in vivo* mouse model of forebrain-specific CIC loss.

Hwang et al. [32] recently showed that CIC functions with the SWI/SNF complex to regulate neuronal differentiation. Our results support and expand these observations into additional cellular contexts, notably demonstrating, for the first time, that CIC physically interacts with the SWI/SNF complex members SMARCA2, SMARCC1, ARID1A, and ARID2 in NHA and HEK cell lines. SMARCA5 and SMARCC2 were further identified as high-confidence candidate interactors in these cell lines. SMARCC1 is a core component found in all SWI/SNF sub-complexes (i.e. BAF, esBAF, nBAF, npBAF, GBAF, and PBAF) [121]. Either SMARCA2 or SMARCA4 is required across all SWI/SNF complexes, although SMARCA2 is excluded from the esBAF and GBAF complexes. ARID1A and ARID2 are mutually exclusive in terms of their sub-complex memberships: ARID1A is found in the BAF, esBAF, nBAF, and npBAFcomplexes, but is excluded from the PBAF and GFAB sub-complexes, while ARID2 is specific to the PBAF subunit. We found that CIC co-localized with ARID1A,

SMARCA2, and SMARCC1 throughout the cell cycle, displaying a dynamic relocalization pattern that included foci formation at de-condensing chromosomes during initiation of nuclear envelope reassembly and accumulation of these foci until completion of cytokinesis. Co-localization between CIC and ARID2, on the other hand, occurred only later on in mitosis, when PBAF, which has been observed to localise to kinetochores and spindle poles in mitotic cells [122], is no longer localised to kinetochores. Our IP-MS and co-localization assays thus indicate that CIC's interaction with ARID1A-, SMARCA2-, and SMARCC1-containing sub-complexes (i.e. BAF, nBAF, and/or npBAF) occurs throughout the cell cycle and mitosis, whereas it does not appear to interact with the ARID2-containing PBAF sub-complex during most of mitosis.

Our co-essentiality and co-expression analyses indicated that CIC may share functionality with BICRA/GLTSCR1, a component of the recently identified non-canonical GBAF SWI/SNF complex [67]. While the fact that *CIC* and *BICRA* reside on the same chromosome arm increases the possibility that the co-essentiality and co-expression relationships we identified between them are false positives [41], our analysis of publicly available ChIP-seq data from mESCs [22,105] indicated that CIC binding sites on the genome overlap with those of SWI/SNF members and provided further support for a potential association between CIC and the GBAF sub-complex. Specifically, we found that CIC binding sites overlapped with those of BRD4, which has been shown to interact with BICRA/GLTSCR1 [67,123] and to recruit the GBAF complex to naive pluripotency genes in mESCs [105], and those of BRD9, which is a required component of the GBAF complex and an optional component of the npBAF and nBAF complexes [121]. Although the nature of the GBAF complex's roles in mammalian development and disease remain poorly understood, early evidence is consistent with the notion that it is a key mediator of these processes [121], warranting further investigation into CIC's potential association with this non-canonical sub-complex. Together, our results build on previous studies to provide multiple additional lines of evidence supporting the notion that CIC interacts with SWI/SNF complexes in several cellular contexts. Given that CIC's transcriptional repressor function was found to be dependent on its interaction with the SWI/SNF

complex during neuronal development [32], our observations indicate the possibility that this cooperative relationship could be at play in additional cellular contexts.

In addition to CIC's interactions with SWI/SNF complexes, another major finding of our study is that CIC appears to play a role in mitotic integrity, as evidenced by the observation that its loss is associated with increased mitotic defects in several *in vitro* and *in vivo* models. Notably, these two observations may be related to one another; indeed, the SWI/SNF complex has been implicated in the maintenance of genomic stability, and disruption of its activity has been associated with mitotic defects similar to the ones we observed in this study, such as faulty chromosome segregation [122,124–126]. The mapping of CIC's genetic and physical interaction networks also revealed several additional interactors involved in cell cycle and mitotic control. For example, *BECN1*, which was predicted to share both co-essentiality and a synthetic lethal partnership with *CIC*, has been shown to promote accurate kinetochore anchoring to mitotic spindles [52] and proper cytokinetic abscission [127], and to regulate autophagy and apoptotic processes [51]. Notably, inhibition of *BECN1* expression is associated with phenotypes similar to the ones we observed in CIC-deficient cells, such as an increased frequency of cytokinesis defects [52]. BECN1's known role in supporting the formation of mitotic structures, together with our failure to observe co-localization between CIC and these structures in mitotic cells, raise the possibility that CIC may be involved in a parallel role that converges with BECN1's function in maintaining mitotic fidelity, which could explain why their combined loss is predicted to be incompatible with cell survival. Further supporting this notion, our analyses of scRNA-seq data identified several genes involved in cell cycle and mitotic checkpoints as being less abundantly expressed in CIC^{KO} cells, indicating the possibility that these checkpoints could be compromised in CIC-deficient cells. For example, the spindle assembly checkpoint (SAC) gene *MAD2L1* was found to be more lowly expressed in G2/M CIC^{KO} cells, and cells with dysregulated SAC function display mitotic defect phenotypes similar to the ones we observed in CIC^{KO} cells, such as an increased incidence of lagging chromosomes and micronuclei [128,129].

Another important finding that emerged from our study is the observation that CIC interacts (both physically and genetically) with a wide range of proteins and genes involved in RNA processing and splicing and mRNA stability. For example, the list of 156 proteins we identified as high-confidence candidate physical interactors of CIC included at least 38 proteins annotated as being involved in functions related to RNA splicing, rRNA/mRNA metabolism and processing, and ribosome biogenesis, which is consistent with the notion that CIC physically interacts with RNA processing complexes. Furthermore, genetic interactions were also observed between *CIC* and genes that play a role in mRNA stability, such as *FXR1*, which has been shown to stabilise transcripts through binding to their 5' or 3' UTRs [55–57] and which was identified as co-essential with *CIC*, and *HNRNPA0*, which can also stabilise transcripts through binding to their 3' UTRs [79] and which was identified as a synthetic lethal partner of *CIC* as well as a high-confidence physical interactor (Supplemental Table S4). Through analysis of bulk RNA-seq data that our group previously generated from *CIC* WT and KO NHA cell lines, we found that loss of CIC is associated with dysregulated splicing specifically at 5' and 3' UTRs, raising the possibility that CIC also plays a role in mRNA stability. Interestingly, SOX2 was recently shown to interact with RNA through its HMG domain [130], raising the intriguing possibility that CIC's conserved HMG domain [131] may also mediate RNA interactions to contribute to splicing regulation.

Many transcription and splicing factors have been implicated in mitotic control, although in most cases it is unclear whether these effects are direct or indirect (e.g. through expression or splicing modulation of dedicated mitotic factors) [132]. Our results indicate that CIC may be one such factor that is involved in transcriptional and splicing regulation as well as mitotic fidelity control, although the latter may be indirect (e.g. through the regulation of mitotic genes, as described above). Again, interactors of CIC identified in our analyses support this notion. For example, CDC5L, a core component of the CDC5L-PRP19 complex that is required for activating pre-mRNA splicing [133], was identified as a high-confidence candidate physical interactor of CIC (Supplemental Table S4). CDC5L knockdown leads to severe mitotic defects and mitotic arrest, phenotypes that have been attributed to defective splicing of

mitotic genes [134]. However, additional studies indicate the possibility that CDC5L also plays a direct role in mitotic spindle assembly, although the exact nature of this role remains unknown (reviewed by Somma et al. [132]). CDC5L is also a component of the *NORAD*-activated ribonucleoprotein complex 1 (NARC1), which additionally contains another protein that we identified as a high-confidence candidate CIC protein interactor, RBMX [135]. Notably, depletion of RBMX was found to be associated with chromosome segregation defects similar to the ones we observed in CIC^{KO} cell lines [135]. Together, these results support the notion that CIC's transcriptional repressor function and its proposed roles in regulation of mitotic fidelity and splicing control may be related, and that these combined functions likely rely on CIC's physical interactions with similar factors and complexes.

It is worth noting that, in addition to the putative novel roles discussed above, our study also reinforced CIC's known role as an effector of MAPK signalling and also provided clues as to interactions between this established function and CIC's possible novel ones. For example, CIC's co-essential network, which is composed of genes with which *CIC* is likely to share functionality, included several known regulators of MAPK signalling, including *DUSP6*, *RASA1*, and *ERF*. Notably, CIC and ERF have been shown to co-regulate the expression of ETV1 in prostate cancer, where their combined loss and subsequent increase in *ETV1* expression contributes to disease progression [66]. *CIC* and *ERF* are located directly adjacent to one another on chromosome 19q13.2 (~14 kb to the long isoform and ~28 kb to the short isoform) and are transcribed in opposing directions. Interestingly, their proximity is conserved in the *mus musculus* genome, where their orthologues *Cic* and *Erf* are both located on chromosome 7 at 13.73cM (~15 kb and ~30 kb apart from the long and short isoform of Cic, respectively). Their proximity suggests that *CIC* and *ERF* may be co-regulated by a shared upstream regulatory factor. As mentioned above, the two genes are co-deleted in 1p/19q co-deleted low-grade gliomas and also frequently in prostate adenocarcinomas (~10-12% of cases) [66], suggesting that the dual loss of CIC and ERF (possibly with GLTSCR1, as discussed above) may favour tumour development, possibly through their combined dysregulation of MAPK signalling. Further studies aimed at distinguishing the joint and

distinct roles of CIC and ERF are thus warranted in order to reveal the extent and implication of their cooperative roles. Our scRNA-seq data also revealed that CIC loss was associated with increased expression of MAPK signalling targets across cell cycle phases, indicating that this function is conserved during mitosis. Interestingly, the MEK-ERK signalling cascade has also been implicated in alternative splicing during T cell activation [136]. Similarly, mutations in *HNRNPA0*, a gene identified as a synthetic lethal interactor of *CIC* that encodes a ribonucleoprotein that was also identified as a high-confidence candidate protein interactor of CIC, have been associated with dysregulation of genes associated with ERK/MAPK signalling, including the known *CIC* targets *ETV4* and *DUSP6*, and with cell cycle progression [137]. Together, these results indicate that CIC may function as an effector of MAPK signalling not just through gene expression regulation but possibly also through regulation of transcript splicing and/or stability.

Conclusions

Overall, our study provides a rigorous exploration of CIC's genetic and proteomic interaction networks and considerably expands our understanding of the diverse cellular processes in which CIC appears to play a role. Beyond the insights it provided into CIC function specifically, this work also presents a model for how multi-omic, network-based analyses that leverage both public and novel datasets can reveal novel and interconnected roles for pleiotropic genes/proteins across cellular and subcellular contexts. For instance, our results raise the intriguing possibility that CIC may be required to ensure faithful mitotic division, and that this function may be related to its interactions with SWI/SNF complexes and/or with RNA processing and spliceosomal complexes. This work thus introduces novel avenues through which CIC can act as a pan-cancer tumour suppressor, and we anticipate that it will catalyse further innovative investigations into this intriguing protein's varied roles.

Methods

Cell culture

The IDH1-stable NHA cell line was obtained from Applied Biological Materials (ABM) Inc (T3022; Richmond, BC, Canada). The HEK293A cell line was obtained from Dr. Gregg Morin (Canada's Michael Smith Genome Sciences Centre, Vancouver, BC, Canada) and authenticated by Genetica DNA Laboratories (Cincinnati, OH, USA). The HOG cell line was obtained from Dr. G. Dawson (The University of Chicago, IL, USA). Cells were cultured in Dulbecco's Modified Eagle Medium (DMEM) supplemented with 10% (v/v) heat-inactivated (HI) FBS (Thermo Fisher Scientific, Waltham, MA, USA). Stable cell lines expressing F-CIC-S, F-CIC-L, or F-vec were cultured in DMEM + 10% HI FBS with Zeocin (Thermo Fisher Scientific) selection. Cell culture was performed in a humidified, 37°C, 5% CO_2 incubator.

CIC knockout cell line generation and expression constructs

CRISPR-Cas9 sgRNA sequences were designed to target exon 2 of the *CIC* gene, and CIC^{KO} lines were established from NHA (NHA-$CIC^{KO\text{-}A2}$ and NHA-$CIC^{KO\text{-}H9}$) and HEK293A (HEK-$CIC^{KO\text{-}A9}$ and HEK-$CIC^{KO\text{-}D10}$) cells as described previously [21]. *CIC* knockout status was verified by western blot and Sanger sequencing. N-terminal FLAG-CIC-short form (FLAG-CIC-S) and long-form (FLAG-CIC-L) plasmids were prepared as described previously [76].

scRNA-seq

Single-cell 3' RNA-seq libraries were generated using the Chromium Single Cell 3′ Library & Gel Bead Kit v1 (10X Genomics, Pleasanton, CA) following the manufacturer's protocol. Full details can be found in the Supplemental Methods.

The CellRanger software was used to create fastq files (cellranger mkfastq with default parameters; v1.2.1) and to perform alignment, filtering, barcode counting, and UMI counting (cellranger count with

default parameters except --expect-cells set to 1000 for all samples; v2.1.1). The CellRanger hg19-3.0.0 reference was used for alignment. Data preprocessing was performed in the R statistical software (v3.5.0) [138], based on the filtered count matrices output by CellRanger. Counts for cells from all samples (7,735 cells) were combined into a single count matrix, and genes detected (UMI > 0) in at least two cells were retained. Normalisation was then applied to all cells using the scran R package [139] (v1.10.1). The *quickCluster* function was used to cluster cells for normalisation (with min.mean = 0.1 as suggested for UMI data), and the resulting clusters were used as input to the *computeSumFactors* function (with min.mean = 0.1). These factors were then used in the *normalise* function of the scater R package (v1.10.0).

Cells were scored for cell cycle phases as described by Macosko et al. [88] and Schwabe et al. [89] using the phase-specific genes identified by Whitfield et al. [87] (Supplemental Table S12). Scores were obtained using the *estimate_Schwabe_stage* function implemented in the tricycle R package [140] (v1.2.1), with default parameters. For the differential expression analysis, differential expression was calculated using the DESeq2 R package [141] with default parameters, either for all NHA-*CIC*^{WT} vs NHA-*CIC*^{KO} samples or for all *CIC*^{WT} samples vs *CIC*^{KO} samples from a single cell line (NHA-*CIC*^{KO1} or NHA-*CIC*^{KO2}). Genes with a BH-corrected *p*-value < 0.1 and an absolute fold-change > 1.5 were considered to be significantly differentially expressed. To visualise these expression differences, DESeq2-normalised expression values were obtained using the *counts* function with normalized = TRUE. By default, DESeq2 performs independent filtering based on mean expression across samples in order to select a set of genes for multiple test correction that maximises the number of genes found at the specified false discovery rate [141]. Therefore, for each differential expression analysis, genes that were detected below the mean cutoff for that comparison were not analysed (returned a corrected *p*-value of “NA”); these comparisons are indicated with “NC” (not calculated) in the relevant figures.

IP-MS

The IP-MS analyses of nuclear fractions from HEK293A cells using anti-endogenous CIC or anti-Myc (for N-Myc-CIC-S) antibodies (Supplemental Table S13) were performed as described previously [76] except using nuclear cell fractions (see Supplemental Methods for more detail). Three replicates were performed against endogenous CIC, and one experiment was performed against N-terminal MYC-fused CIC stably expressed in HEK293A cells. The IP-MS validation experiments performed in nuclear fractions of the NHA cell line were performed in triplicate, as were the matched IgG controls. See Supplemental Methods for methodological details.

Co-essentiality mapping and in silico genetic screening framework

Co-essentiality mapping and *in silico* genetic interaction screening were performed using the R statistical software (v4.0.2) package GRETA (v0.5.0) [142], with DepMap public release version 20Q1 [40] data from the DepMap platform portal (https://depmap.org/portal/download/). Briefly, co-essentiality mapping uses fitness effect scores that were derived from normalised and copy number-corrected whole-genome CRISPR-Cas9 knockout screens targeting 18,333 genes performed in 739 cancer cell lines [38,39]. GRETA calculates and ranks Pearson correlation coefficients between fitness scores of *CIC* and each screened gene, and a gene pair was considered co-essential if its BH-adjusted p-value was < 0.05 and its coefficient was > 0.178 (the inflection point).

Using GRETA, *CIC*-mutant lines were identified using genomic data from 739 DepMap cancer cell lines. We identified two lines (HCC366 and JHUEM1) with homozygous deleterious *CIC* alterations (CIC^{HomDel}), five lines (REH, CCK81, HEC6, GP4D, and SISO) with potentially trans-heterozygous *CIC* mutations ($CIC^{T\text{-}HetDel}$; multiple heterozygous deleterious *CIC* mutations or a combination of partial copy number loss with heterozygous deleterious *CIC* mutation[s]), 53 lines with a single heterozygous deleterious *CIC* mutation or partial copy number loss (CIC^{HetDel}), and 557 lines with no *CIC* alterations

(*CIC*^{WT}; Supplemental Table S2). The normalised TPM gene and protein expression values for the selected cell lines were extracted using GRETA.

Pairwise Mann-Whitney U tests between *CIC* mutant and *CIC*^{WT} cell lines for all 18,333 genes were performed using GRETA to obtain p-values. These p-values were adjusted for multiple testing using a permutation approach, whereby the lethality probabilities were randomised and resampled 10,000 times. Candidate genetic interactors of *CIC* that were identified using *CIC*^{HomDel} mutant cell lines were defined as those with an adjusted Mann-Whitney U test p-value < 0.05 and a median lethality probability > 0.5 in at least one group. Known essential and non-essential genes, as defined by DepMap, were filtered out.

Co-expression analysis

Genes co-expressed with CIC were downloaded from COXPRESdb (v8.1) [59]. COXPRESdb is a database that was previously used by Pan et al. [143] and Wainberg et al. [41] to benchmark co-essential genes. The database contains co-expression z-scores between *CIC* and 17,067 genes from over 10,485 human samples assayed using RNA-seq ("hsa-r.6"), where a z-score of zero is a random level, and a score of three is a false positive rate of 0.1% for any species or version. In this study, we used the top 50 genes co-expressed with CIC.

ChIP-seq analysis

CIC ChIP-seq peaks for NHA cells were obtained from Lee et al. [24] (Table S3 in that publication). ChIP-seq data from mESCs (fastq files) were downloaded from ArrayExpress (ERR2534130 [CIC ChIP] and ERR2534131 [IgG control], data from Weissmann et al. [22]) and SRA (SRR7643337 [ARID1A ChIP replicate 1], SRR7643339 [ARID1A input control replicate 1], SRR7643338 [ARID1A ChIP replicate 2], SRR7643340 [ARID1A input control replicate 2], SRR7643346 [BRD4 ChIP], SRR7643347 [BRD4 input control], SRR6792731 [BRD9 ChIP], SRR6792735 [BRD9 input control], SRR7724001 [SMARCA4 ChIP], SRR7724002 [SMARCA4 input control], data from Gatchalian et al. [105]).

Alignments were performed using BWA (v0.7.17) [144] using the mm10 genome as a reference. Aligned read files were sorted and indexed using samtools (v1.9) [145,146]. Peaks were called using MACS2 (v2.1.1) [147] using the input files as controls and default parameters. For ARID1A, peaks that were identified in both replicates (≥ 1 base overlap) were retained for downstream analyses. Peaks were annotated using the *annotatePeak* function from the ChIPseeker R package (v1.30.3) [148,149] using the *TxDb.Mmusculus.UCSC.mm10.knownGene* annotation from the R package of the same name (v3.10.0). The *findOverlaps* function from the GenomicRanges R package (v1.46.1) [150] was used to identify CIC peaks that overlapped with one or more SWI/SNF peaks. Hypergeometric tests were used to quantify the statistical significance of peak overlaps, as implemented in the *makeVennDiagram* function of the ChIPpeakAnno R package (v3.28.1) [151,152]. The *totalTest* argument was set to 250,000, as recommended by the authors for stem cell datasets.

Alternative splicing quantification

Alternative splicing events analysed using Whippet v1.6.1 [106] and run on Julia v1.8.0. Bulk RNAseq .fastq files were used as input to quantify splicing events using the whippet-quant.jl function with the options --stranded, --circ, and --biascorrect, and to generate .sam files for visualisation using the --sam option. Differential splicing events were quantified using the whippet-delta.jl function with default options. Splicing events were visualised using IGV v2.8.13 [153] after .sam files were converted to .bam files using samtools v1.9 [146].

Declarations

Funding

This study was supported in part by the Canadian Institutes of Health Research (CIHR; FDN-143288).

Acknowledgements

The authors thank the Sequencing, Bioinformatics, and Project Management teams at Canada's Michael Smith Genome Sciences Centre for expert technical contributions. We thank Dr. Michel Roberge and Dr. Phil Hieter for helpful edits and comments on early versions of the manuscript and Dr. G. Dawson for providing the HOG cell line. We are especially grateful to Ms Donna Anderson for her generosity in supporting this project through the UBC Foundation. MAM gratefully acknowledges the support of BC Cancer, the BC Cancer Foundation, the Canada Research Chairs program, the Canada Foundation for Innovation (projects 20070, 30981, and 33408), Genome BC, Genome Canada, and the University of British Columbia (UBC). VGL was supported by a CIHR Vanier Canada Graduate Scholarship and a Killam Doctoral Scholarship. YT and VGL were supported by UBC 4-year fellowships. YT was supported by UBC international student awards, and UBC President's Academic Excellence Initiative PhD Awards.

Author contributions

Conceptualization, MAM, YT, VGL, and SC; Methodology, MAM, YT, VGL, and SC; Software, YT, VGL, and CSH; Validation, YT, VGL, SC, JS, SYC, SAJRA, SMG; Formal Analysis, YT, VGL, and SC; Investigation, SC, JS, SYC, SDL, YT, AG, DLT, WRB, AM, CSH, and GBM.; Resources, SC, JS, SYC, STA, CSH, JGC, JAC, GBM, SAJRA, SMG, MAM; Data Curation, YT, VGL, CSH, RDC, and SC; Writing – Original Draft Preparation, YT, VGL, SC; Writing – Review & Editing, YT, VGL, MAM, DLT, RDC, JAC, SAA, SMG, GBM, JGC, and SY; Visualization, YT, VGL, SC, JS, SYC; Supervision, MAM; Project Administration, YT, VGL, SC, MAM; Funding Acquisition, MAM.

Institutional review board statement

Animal use was approved by the University of Calgary Animal Care Committee (protocol AC16-0266) in compliance with the Guidelines of the Canadian Council of Animal Care. The work presented here was approved by the UBC BC Cancer Research Ethics Board (H19-03010, H08-02838).

Data availability statement

scRNA-seq data have been deposited in the Gene Expression Omnibus (GEO; accession GSE193765). IP-MS data have been deposited to the ProteomeXchange Consortium via the Proteomics Identification (PRIDE) database [154] (accession PXD030942).

Conflicts of interest

SY is a member of the advisory boards of Amgen, AstraZeneca, Bayer, Incyte, and Roche. SAA is a co-founder of and consultant to Contextual Genomics Ltd and is on the advisory boards of Sangamo Biosciences and Repare Therapeutics. The remaining authors declare no competing interests.

References

1. Haidar, A.; Arekapudi, S.; DeMattia, F.; Abu-Isa, E.; Kraut, M. High-Grade Undifferentiated Small Round Cell Sarcoma with t(4;19)(q35;q13.1) CIC-DUX4 Fusion: Emerging Entities of Soft Tissue Tumors with Unique Histopathologic Features--a Case Report and Literature Review. *Am. J. Case Rep.* **2015**, *16*, 87–94, doi:10.12659/AJCR.892551.
2. Bettegowda, C.; Agrawal, N.; Jiao, Y.; Sausen, M.; Wood, L.D.; Hruban, R.H.; Rodriguez, F.J.; Cahill, D.P.; McLendon, R.; Riggins, G.; et al. Mutations in CIC and FUBP1 Contribute to Human Oligodendroglioma. *Science* **2011**, *333*, 1453–1455, doi:10.1126/science.1210557.
3. Yip, S.; Butterfield, Y.S.; Morozova, O.; Chittaranjan, S.; Blough, M.D.; An, J.; Birol, I.; Chesnelong, C.; Chiu, R.; Chuah, E.; et al. Concurrent CIC Mutations, IDH Mutations, and 1p/19q Loss Distinguish Oligodendrogliomas from Other Cancers. *J. Pathol.* **2012**, *226*, 7–16, doi:10.1002/path.2995.
4. The Cancer Genome Atlas Research Network, Comprehensive Molecular Characterization of Gastric Adenocarcinoma. *Nature* **2014**, *513*, 202–209, doi:10.1038/nature13480.
5. The Cancer Genome Atlas Research Network, Integrated Genomic Characterization of Endometrial Carcinoma. *Nature* **2013**, *497*, 67–73, doi:10.1038/nature12113.
6. Cerami, E.; Gao, J.; Dogrusoz, U.; Gross, B.E.; Sumer, S.O.; Aksoy, B.A.; Jacobsen, A.; Byrne, C.J.; Heuer, M.L.; Larsson, E.; et al. The cBio Cancer Genomics Portal: An Open Platform for Exploring Multidimensional Cancer Genomics Data. *Cancer Discov.* **2012**, *2*, 401–404, doi:10.1158/2159-8290.CD-12-0095.
7. Gao, J.; Aksoy, B.A.; Dogrusoz, U.; Dresdner, G.; Gross, B.; Sumer, S.O.; Sun, Y.; Jacobsen, A.; Sinha, R.; Larsson, E.; et al. Integrative Analysis of Complex Cancer Genomics and Clinical Profiles Using the cBioPortal. *Sci. Signal.* **2013**, *6*, l1, doi:10.1126/scisignal.2004088.
8. Choi, N.; Park, J.; Lee, J.S.; Yoe, J.; Park, G.Y.; Kim, E.; Jeon, H.; Cho, Y.M.; Roh, T.Y.; Lee, Y. miR-93/miR-106b/miR-375-CIC-CRABP1: A Novel Regulatory Axis in Prostate Cancer Progression. *Oncotarget* **2015**, *6*, 23533–23547.
9. Okimoto, R.A.; Breitenbuecher, F.; Olivas, V.R.; Wu, W.; Gini, B.; Hofree, M.; Asthana, S.; Hrustanovic, G.; Flanagan, J.; Tulpule, A.; et al. Inactivation of Capicua Drives Cancer Metastasis. *Nat. Genet.* **2017**, *49*, 87–96, doi:10.1038/ng.3728.
10. Simon-Carrasco, L.; Grana, O.; Salmon, M.; Jacob, H.K.C.; Gutierrez, A.; Jimenez, G.; Drosten, M.; Barbacid, M. Inactivation of Capicua in Adult Mice Causes T-Cell Lymphoblastic Lymphoma. *Genes Dev.* **2017**, doi:10.1101/gad.300244.117.
11. Tan, Q.; Brunetti, L.; Rousseaux, M.W.C.; Lu, H.C.; Wan, Y.W.; Revelli, J.P.; Liu, Z.; Goodell, M.A.; Zoghbi, H.Y. Loss of Capicua Alters Early T Cell Development and Predisposes Mice to T Cell Lymphoblastic Leukemia/lymphoma. *Proc. Natl. Acad. Sci. U. S. A.* **2018**, doi:10.1073/pnas.1716452115.
12. Chan, A.K.; Pang, J.C.; Chung, N.Y.; Li, K.K.; Poon, W.S.; Chan, D.T.; Shi, Z.; Chen, L.; Zhou, L.; Ng, H.K. Loss of CIC and FUBP1 Expressions Are Potential Markers of Shorter Time to Recurrence in Oligodendroglial Tumors. *Mod. Pathol.* **2014**, *27*, 332–342, doi:10.1038/modpathol.2013.165.
13. Gleize, V.; Alentorn, A.; Connen de Kerillis, L.; Labussiere, M.; Nadaradjane, A.; Mundwiller, E.; Ottolenghi, C.; Mangesius, S.; Rahimian, A.; Ducray, F.; et al. CIC Inactivating Mutations Identify Aggressive Subset of 1p19q Codeleted Gliomas. *Ann. Neurol.* **2015**, *78*, 355–374, doi:10.1002/ana.24443.
14. Specht, K.; Sung, Y.S.; Zhang, L.; Richter, G.H.; Fletcher, C.D.; Antonescu, C.R. Distinct Transcriptional Signature and Immunoprofile of CIC-DUX4 Fusion-Positive Round Cell Tumors Compared to EWSR1-Rearranged Ewing Sarcomas: Further Evidence toward Distinct Pathologic Entities. *Genes Chromosomes Cancer* **2014**, *53*, 622–633, doi:10.1002/gcc.22172.
15. Antonescu, C.R.; Owosho, A.A.; Zhang, L.; Chen, S.; Deniz, K.; Huryn, J.M.; Kao, Y.C.; Huang,

S.C.; Singer, S.; Tap, W.; et al. Sarcomas With CIC-Rearrangements Are a Distinct Pathologic Entity With Aggressive Outcome: A Clinicopathologic and Molecular Study of 115 Cases. *Am. J. Surg. Pathol.* **2017**, doi:10.1097/PAS.0000000000000846.
16. Liao, S.; Davoli, T.; Leng, Y.; Li, M.Z.; Xu, Q.; Elledge, S.J. A Genetic Interaction Analysis Identifies Cancer Drivers That Modify EGFR Dependency. *Genes Dev.* **2017**, *31*, 184–196, doi:10.1101/gad.291948.116.
17. Wang, B.; Krall, E.B.; Aguirre, A.J.; Kim, M.; Widlund, H.R.; Doshi, M.B.; Sicinska, E.; Sulahian, R.; Goodale, A.; Cowley, G.S.; et al. ATXN1L, CIC, and ETS Transcription Factors Modulate Sensitivity to MAPK Pathway Inhibition. *Cell Rep.* **2017**, *18*, 1543–1557, doi:10.1016/j.celrep.2017.01.031.
18. Hashiba, T.; Yamashita, T.; Okada, H.; Nio, K.; Hayashi, T.; Asahina, Y.; Hayashi, T.; Terashima, T.; Iida, N.; Takatori, H.; et al. Inactivation of Transcriptional Repressor Capicua Confers Sorafenib Resistance in Human Hepatocellular Carcinoma. *Cell Mol Gastroenterol Hepatol* **2020**, *10*, 269–285, doi:10.1016/j.jcmgh.2020.02.009.
19. Simón-Carrasco, L.; Jiménez, G.; Barbacid, M.; Drosten, M. The Capicua Tumor Suppressor: A Gatekeeper of Ras Signaling in Development and Cancer. *Cell Cycle* **2018**, *17*, 702–711, doi:10.1080/15384101.2018.1450029.
20. Padul, V.; Epari, S.; Moiyadi, A.; Shetty, P.; Shirsat, N.V. ETV/Pea3 Family Transcription Factor-Encoding Genes Are Overexpressed in CIC-Mutant Oligodendrogliomas. *Genes Chromosomes Cancer* **2015**, *54*, 725–733, doi:10.1002/gcc.22283.
21. LeBlanc, V.G.; Firme, M.; Song, J.; Chan, S.Y.; Lee, M.H.; Yip, S.; Chittaranjan, S.; Marra, M.A. Comparative Transcriptome Analysis of Isogenic Cell Line Models and Primary Cancers Links CIC Loss to Activation of the MAPK Signalling Cascade. *J. Pathol.* **2017**, doi:10.1002/path.4894.
22. Weissmann, S.; Cloos, P.A.; Sidoli, S.; Jensen, O.N.; Pollard, S.; Helin, K. The Tumor Suppressor CIC Directly Regulates MAPK Pathway Genes via Histone Deacetylation. *Cancer Res.* **2018**, *78*, 4114–4125, doi:10.1158/0008-5472.CAN-18-0342.
23. Ren, Y.; Ouyang, Z.; Hou, Z.; Yan, Y.; Zhi, Z.; Shi, M.; Du, M.; Liu, H.; Wen, Y.; Shao, Y. CIC Is a Mediator of the ERK1/2-DUSP6 Negative Feedback Loop. *iScience* **2020**, *23*, 101635, doi:10.1016/j.isci.2020.101635.
24. Lee, S.D.; Song, J.; LeBlanc, V.G.; Marra, M.A. Integrative Multi-Omic Analysis Reveals Neurodevelopmental Gene Dysregulation in CIC-Knockout and IDH1-Mutant Cells. *J. Pathol.* **2022**, *256*, 297–309, doi:10.1002/path.5835.
25. Jimenez, G.; Shvartsman, S.Y.; Paroush, Z. The Capicua Repressor--a General Sensor of RTK Signaling in Development and Disease. *J. Cell Sci.* **2012**, *125*, 1383–1391, doi:10.1242/jcs.092965.
26. Tseng, A.S.; Tapon, N.; Kanda, H.; Cigizoglu, S.; Edelmann, L.; Pellock, B.; White, K.; Hariharan, I.K. Capicua Regulates Cell Proliferation Downstream of the Receptor Tyrosine Kinase/ras Signaling Pathway. *Curr. Biol.* **2007**, *17*, 728–733, doi:10.1016/j.cub.2007.03.023.
27. Jin, Y.; Ha, N.; Fores, M.; Xiang, J.; Glasser, C.; Maldera, J.; Jimenez, G.; Edgar, B.A. EGFR/Ras Signaling Controls Drosophila Intestinal Stem Cell Proliferation via Capicua-Regulated Genes. *PLoS Genet.* **2015**, *11*, e1005634, doi:10.1371/journal.pgen.1005634.
28. Yang, R.; Chen, L.H.; Hansen, L.J.; Carpenter, A.B.; Moure, C.J.; Liu, H.; Pirozzi, C.J.; Diplas, B.H.; Waitkus, M.S.; Greer, P.K.; et al. Cic Loss Promotes Gliomagenesis via Aberrant Neural Stem Cell Proliferation and Differentiation. *Cancer Res.* **2017**, *77*, 6097–6108, doi:10.1158/0008-5472.CAN-17-1018.
29. Wong, D.; Lounsbury, K.; Lum, A.; Song, J.; Chan, S.; LeBlanc, V.; Chittaranjan, S.; Marra, M.; Yip, S. Transcriptomic Analysis of CIC and ATXN1L Reveal a Functional Relationship Exploited by Cancer. *Oncogene* **2019**, *38*, 273–290, doi:10.1038/s41388-018-0427-5.
30. Lee, Y. Regulation and Function of Capicua in Mammals. *Exp. Mol. Med.* **2020**, *52*, 531–537, doi:10.1038/s12276-020-0411-3.

31. Lam, Y.C.; Bowman, A.B.; Jafar-Nejad, P.; Lim, J.; Richman, R.; Fryer, J.D.; Hyun, E.D.; Duvick, L.A.; Orr, H.T.; Botas, J.; et al. ATAXIN-1 Interacts with the Repressor Capicua in Its Native Complex to Cause SCA1 Neuropathology. *Cell* **2006**, *127*, 1335–1347, doi:10.1016/j.cell.2006.11.038.
32. Hwang, I.; Pan, H.; Yao, J.; Elemento, O.; Zheng, H.; Paik, J. CIC Is a Critical Regulator of Neuronal Differentiation. *JCI Insight* **2020**, *5*, doi:10.1172/jci.insight.135826.
33. VanderSluis, B.; Costanzo, M.; Billmann, M.; Ward, H.N.; Myers, C.L.; Andrews, B.J.; Boone, C. Integrating Genetic and Protein-Protein Interaction Networks Maps a Functional Wiring Diagram of a Cell. *Curr. Opin. Microbiol.* **2018**, *45*, 170–179, doi:10.1016/j.mib.2018.06.004.
34. Takemon, Y.; Chick, J.M.; Gerdes Gyuricza, I.; Skelly, D.A.; Devuyst, O.; Gygi, S.P.; Churchill, G.A.; Korstanje, R. Proteomic and Transcriptomic Profiling Reveal Different Aspects of Aging in the Kidney. *Elife* **2021**, *10*, doi:10.7554/eLife.62585.
35. Shan, G.; Zhang, H.; Bi, G.; Bian, Y.; Liang, J.; Valeria, B.; Zeng, D.; Yao, G.; Zhan, C.; Fan, H. Multi-Omics Analysis of Cancer Cell Lines with High/Low Ferroptosis Scores and Development of a Ferroptosis-Related Model for Multiple Cancer Types. *Front Cell Dev Biol* **2021**, *9*, 794475, doi:10.3389/fcell.2021.794475.
36. Pan, J.; Meyers, R.M.; Michel, B.C.; Mashtalir, N.; Sizemore, A.E.; Wells, J.N.; Cassel, S.H.; Vazquez, F.; Weir, B.A.; Hahn, W.C.; et al. Interrogation of Mammalian Protein Complex Structure, Function, and Membership Using Genome-Scale Fitness Screens. *Cell Syst* **2018**, *6*, 555–568.e7, doi:10.1016/j.cels.2018.04.011.
37. Michel, B.C.; D'Avino, A.R.; Cassel, S.H.; Mashtalir, N.; McKenzie, Z.M.; McBride, M.J.; Valencia, A.M.; Zhou, Q.; Bocker, M.; Soares, L.M.M.; et al. A Non-Canonical SWI/SNF Complex Is a Synthetic Lethal Target in Cancers Driven by BAF Complex Perturbation. *Nat. Cell Biol.* **2018**, *20*, 1410–1420, doi:10.1038/s41556-018-0221-1.
38. Meyers, R.M.; Bryan, J.G.; McFarland, J.M.; Weir, B.A.; Sizemore, A.E.; Xu, H.; Dharia, N.V.; Montgomery, P.G.; Cowley, G.S.; Pantel, S.; et al. Computational Correction of Copy Number Effect Improves Specificity of CRISPR-Cas9 Essentiality Screens in Cancer Cells. *Nat. Genet.* **2017**, *49*, 1779–1784, doi:10.1038/ng.3984.
39. Dempster, J.M.; Rossen, J.; Kazachkova, M.; Pan, J.; Kugener, G.; Root, D.E.; Tsherniak, A. Extracting Biological Insights from the Project Achilles Genome-Scale CRISPR Screens in Cancer Cell Lines 2019, 720243.
40. DepMap, B. DepMap 20Q1 Public 2020.
41. Wainberg, M.; Kamber, R.A.; Balsubramani, A.; Meyers, R.M.; Sinnott-Armstrong, N.; Hornburg, D.; Jiang, L.; Chan, J.; Jian, R.; Gu, M.; et al. A Genome-Wide Atlas of Co-Essential Modules Assigns Function to Uncharacterized Genes. *Nat. Genet.* **2021**, *53*, 638–649, doi:10.1038/s41588-021-00840-z.
42. Zhang, Y.; Li, Y.; Wang, Q.; Su, B.; Xu, H.; Sun, Y.; Sun, P.; Li, R.; Peng, X.; Cai, J. Role of RASA1 in Cancer: A Review and Update (Review). *Oncol. Rep.* **2020**, *44*, 2386–2396, doi:10.3892/or.2020.7807.
43. Benatti, P.; Dolfini, D.; Viganò, A.; Ravo, M.; Weisz, A.; Imbriano, C. Specific Inhibition of NF-Y Subunits Triggers Different Cell Proliferation Defects. *Nucleic Acids Res.* **2011**, *39*, 5356–5368, doi:10.1093/nar/gkr128.
44. Moeinvaziri, F.; Shahhoseini, M. Epigenetic Role of CCAAT Box-Binding Transcription Factor NF-Y on ID Gene Family in Human Embryonic Carcinoma Cells. *IUBMB Life* **2015**, *67*, 880–887, doi:10.1002/iub.1443.
45. Jongsma, M.L.M.; de Waard, A.A.; Raaben, M.; Zhang, T.; Cabukusta, B.; Platzer, R.; Blomen, V.A.; Xagara, A.; Verkerk, T.; Bliss, S.; et al. The SPPL3-Defined Glycosphingolipid Repertoire Orchestrates HLA Class I-Mediated Immune Responses. *Immunity* **2021**, *54*, 132–150.e9, doi:10.1016/j.immuni.2020.11.003.

46. Park, S.; Lee, S.; Lee, C.G.; Park, G.Y.; Hong, H.; Lee, J.S.; Kim, Y.M.; Lee, S.B.; Hwang, D.; Choi, Y.S.; et al. Capicua Deficiency Induces Autoimmunity and Promotes Follicular Helper T Cell Differentiation via Derepression of ETV5. *Nat. Commun.* **2017**, *8*, 16037, doi:10.1038/ncomms16037.
47. Park, S.; Park, J.; Kim, E.; Lee, Y. The Capicua-ETV5 Axis Regulates Liver-Resident Memory CD8(+) T Cell Development and the Pathogenesis of Liver Injury. *Hepatology* **2019**, doi:10.1002/hep.30594.
48. Park, G.-Y.; Lee, G.-W.; Kim, S.; Hong, H.; Park, J.S.; Cho, J.-H.; Lee, Y. Deletion Timing of Cic Alleles during Hematopoiesis Determines the Degree of Peripheral CD4+ T Cell Activation and Proliferation. *Immune Netw.* **2020**, *20*, e43, doi:10.4110/in.2020.20.e43.
49. Kim, S.; Park, G.-Y.; Park, J.S.; Park, J.; Hong, H.; Lee, Y. Regulation of Positive and Negative Selection and TCR Signaling during Thymic T Cell Development by Capicua. *Elife* **2021**, *10*, doi:10.7554/eLife.71769.
50. Li, H.; Liu, Q.; Hu, X.; Feng, D.; Xiang, S.; He, Z.; Hu, X.; Zhou, J.; Ding, X.; Zhou, C.; et al. Human ZCCHC12 Activates AP-1 and CREB Signaling as a Transcriptional Co-Activator. *Acta Biochim. Biophys. Sin.* **2009**, *41*, 535–544, doi:10.1093/abbs/gmp042.
51. Kang, R.; Zeh, H.J.; Lotze, M.T.; Tang, D. The Beclin 1 Network Regulates Autophagy and Apoptosis. *Cell Death Differ.* **2011**, *18*, 571–580, doi:10.1038/cdd.2010.191.
52. Frémont, S.; Gérard, A.; Galloux, M.; Janvier, K.; Karess, R.E.; Berlioz-Torrent, C. Beclin-1 Is Required for Chromosome Congression and Proper Outer Kinetochore Assembly. *EMBO Rep.* **2013**, *14*, 364–372, doi:10.1038/embor.2013.23.
53. Cui, Z.; Shen, Y.; Chen, K.H.; Mittal, S.K.; Yang, J.-Y.; Zhang, G. KANK1 Inhibits Cell Growth by Inducing Apoptosis through Regulating CXXC5 in Human Malignant Peripheral Nerve Sheath Tumors. *Sci. Rep.* **2017**, *7*, 40325, doi:10.1038/srep40325.
54. Chen, N.-P.; Sun, Z.; Fässler, R. The Kank Family Proteins in Adhesion Dynamics. *Curr. Opin. Cell Biol.* **2018**, *54*, 130–136, doi:10.1016/j.ceb.2018.05.015.
55. Deng, M.; Wang, N.; Li, Z.; Chen, R.; Duan, J.; Peng, Y.; Wu, Z.; Zhang, Z.; Jiang, L.; Zheng, X.; et al. FXR1 Can Bind with the CFIm25/CFIm68 Complex and Promote the Progression of Urothelial Carcinoma of the Bladder by Stabilizing TRAF1 mRNA. *Cell Death Dis.* **2022**, *13*, 170, doi:10.1038/s41419-022-04614-1.
56. George, J.; Li, Y.; Kadamberi, I.P.; Parashar, D.; Tsaih, S.-W.; Gupta, P.; Geethadevi, A.; Chen, C.; Ghosh, C.; Sun, Y.; et al. RNA-Binding Protein FXR1 Drives cMYC Translation by Recruiting eIF4F Complex to the Translation Start Site. *Cell Rep.* **2021**, *37*, 109934, doi:10.1016/j.celrep.2021.109934.
57. Davidovic, L.; Durand, N.; Khalfallah, O.; Tabet, R.; Barbry, P.; Mari, B.; Sacconi, S.; Moine, H.; Bardoni, B. A Novel Role for the RNA-Binding Protein FXR1P in Myoblasts Cell-Cycle Progression by Modulating p21/Cdkn1a/Cip1/Waf1 mRNA Stability. *PLoS Genet.* **2013**, *9*, e1003367, doi:10.1371/journal.pgen.1003367.
58. van Dam, S.; Võsa, U.; van der Graaf, A.; Franke, L.; de Magalhães, J.P. Gene Co-Expression Analysis for Functional Classification and Gene-Disease Predictions. *Brief. Bioinform.* **2018**, *19*, 575–592, doi:10.1093/bib/bbw139.
59. Obayashi, T.; Kagaya, Y.; Aoki, Y.; Tadaka, S.; Kinoshita, K. COXPRESdb v7: A Gene Coexpression Database for 11 Animal Species Supported by 23 Coexpression Platforms for Technical Evaluation and Evolutionary Inference. *Nucleic Acids Res.* **2019**, *47*, D55–D62, doi:10.1093/nar/gky1155.
60. Reinhard, N.R.; Van Der Niet, S.; Chertkova, A.; Postma, M.; Hordijk, P.L.; Gadella, T.W.J., Jr; Goedhart, J. Identification of Guanine Nucleotide Exchange Factors That Increase Cdc42 Activity in Primary Human Endothelial Cells. *Small GTPases* **2021**, *12*, 226–240, doi:10.1080/21541248.2019.1658509.

61. Chou, M.M.; Masuda-Robens, J.M.; Gupta, M.L. Cdc42 Promotes G1 Progression through p70 S6 Kinase-Mediated Induction of Cyclin E Expression *. *J. Biol. Chem.* **2003**, *278*, 35241–35247, doi:10.1074/jbc.M305246200.
62. Yasuda, S.; Taniguchi, H.; Oceguera-Yanez, F.; Ando, Y.; Watanabe, S.; Monypenny, J.; Narumiya, S. An Essential Role of Cdc42-like GTPases in Mitosis of HeLa Cells. *FEBS Lett.* **2006**, *580*, 3375–3380, doi:10.1016/j.febslet.2006.05.009.
63. Le Gallic, L.; Virgilio, L.; Cohen, P.; Biteau, B.; Mavrothalassitis, G. ERF Nuclear Shuttling, a Continuous Monitor of Erk Activity That Links It to Cell Cycle Progression. *Mol. Cell. Biol.* **2004**, *24*, 1206–1218, doi:10.1128/MCB.24.3.1206-1218.2004.
64. Twigg, S.R.F.; Vorgia, E.; McGowan, S.J.; Peraki, I.; Fenwick, A.L.; Sharma, V.P.; Allegra, M.; Zaragkoulias, A.; Akha, E.S.; Knight, S.J.L.; et al. Reduced Dosage of ERF Causes Complex Craniosynostosis in Humans and Mice and Links ERK1/2 Signaling to Regulation of Osteogenesis. *Nat. Genet.* **2013**, *45*, 308–313, doi:10.1038/ng.2539.
65. Singh, R.; Cohen, A.S.A.; Poulton, C.; Hjortshøj, T.D.; Akahira-Azuma, M.; Mendiratta, G.; Khan, W.A.; Azmanov, D.N.; Woodward, K.J.; Kirchhoff, M.; et al. Deletion of ERF and CIC Causes Abnormal Skull Morphology and Global Developmental Delay. *Cold Spring Harb Mol Case Stud* **2021**, *7*, doi:10.1101/mcs.a005991.
66. Gupta, N.; Song, H.; Wu, W.; Ponce, R.K.; Lin, Y.K.; Kim, J.W.; Small, E.J.; Feng, F.Y.; Huang, F.W.; Okimoto, R.A. The CIC-ERF Co-Deletion Underlies Fusion-Independent Activation of ETS Family Member, ETV1, to Drive Prostate Cancer Progression. *Elife* **2022**, *11*, doi:10.7554/eLife.77072.
67. Alpsoy, A.; Dykhuizen, E.C. Glioma Tumor Suppressor Candidate Region Gene 1 (GLTSCR1) and Its Paralog GLTSCR1-like Form SWI/SNF Chromatin Remodeling Subcomplexes. *J. Biol. Chem.* **2018**, *293*, 3892–3903, doi:10.1074/jbc.RA117.001065.
68. Yue, J.; López, J.M. Understanding MAPK Signaling Pathways in Apoptosis. *Int. J. Mol. Sci.* **2020**, *21*, doi:10.3390/ijms21072346.
69. Guo, Y.-J.; Pan, W.-W.; Liu, S.-B.; Shen, Z.-F.; Xu, Y.; Hu, L.-L. ERK/MAPK Signalling Pathway and Tumorigenesis. *Exp. Ther. Med.* **2020**, *19*, 1997–2007, doi:10.3892/etm.2020.8454.
70. Ghandi, M.; Huang, F.W.; Jané-Valbuena, J.; Kryukov, G.V.; Lo, C.C.; McDonald, E.R., 3rd; Barretina, J.; Gelfand, E.T.; Bielski, C.M.; Li, H.; et al. Next-Generation Characterization of the Cancer Cell Line Encyclopedia. *Nature* **2019**, *569*, 503–508, doi:10.1038/s41586-019-1186-3.
71. Nusinow, D.P.; Szpyt, J.; Ghandi, M.; Rose, C.M.; McDonald, E.R., 3rd; Kalocsay, M.; Jané-Valbuena, J.; Gelfand, E.; Schweppe, D.K.; Jedrychowski, M.; et al. Quantitative Proteomics of the Cancer Cell Line Encyclopedia. *Cell* **2020**, *180*, 387–402.e16, doi:10.1016/j.cell.2019.12.023.
72. Behan, F.M.; Iorio, F.; Picco, G.; Gonçalves, E.; Beaver, C.M.; Migliardi, G.; Santos, R.; Rao, Y.; Sassi, F.; Pinnelli, M.; et al. Prioritization of Cancer Therapeutic Targets Using CRISPR–Cas9 Screens. *Nature* **2019**, *568*, 511–516, doi:10.1038/s41586-019-1103-9.
73. Nijman, S.M. Synthetic Lethality: General Principles, Utility and Detection Using Genetic Screens in Human Cells. *FEBS Lett.* **2011**, *585*, 1–6, doi:10.1016/j.febslet.2010.11.024.
74. van Leeuwen, J.; Boone, C.; Andrews, B.J. Mapping a Diversity of Genetic Interactions in Yeast. *Curr Opin Syst Biol* **2017**, *6*, 14–21, doi:10.1016/j.coisb.2017.08.002.
75. Mashtalir, N.; D'Avino, A.R.; Michel, B.C.; Luo, J.; Pan, J.; Otto, J.E.; Zullow, H.J.; McKenzie, Z.M.; Kubiak, R.L.; St Pierre, R.; et al. Modular Organization and Assembly of SWI/SNF Family Chromatin Remodeling Complexes. *Cell* **2018**, *175*, 1272–1288 e20, doi:10.1016/j.cell.2018.09.032.
76. Chittaranjan, S.; Chan, S.; Yang, C.; Yang, K.C.; Chen, V.; Moradian, A.; Firme, M.; Song, J.; Go, N.E.; Blough, M.D.; et al. Mutations in CIC and IDH1 Cooperatively Regulate 2-Hydroxyglutarate Levels and Cell Clonogenicity. *Oncotarget* **2014**, *5*, 7960–7979.
77. Sonoda, Y.; Ozawa, T.; Hirose, Y.; Aldape, K.D.; McMahon, M.; Berger, M.S.; Pieper, R.O. Formation of Intracranial Tumors by Genetically Modified Human Astrocytes Defines Four

Pathways Critical in the Development of Human Anaplastic Astrocytoma. *Cancer Res.* **2001**, *61*, 4956–4960.
78. Erickson, B.K.; Rose, C.M.; Braun, C.R.; Erickson, A.R.; Knott, J.; McAlister, G.C.; Wühr, M.; Paulo, J.A.; Everley, R.A.; Gygi, S.P. A Strategy to Combine Sample Multiplexing with Targeted Proteomics Assays for High-Throughput Protein Signature Characterization. *Mol. Cell* **2017**, *65*, 361–370, doi:10.1016/j.molcel.2016.12.005.
79. Reinhardt, H.C.; Hasskamp, P.; Schmedding, I.; Morandell, S.; van Vugt, M.A.T.M.; Wang, X.; Linding, R.; Ong, S.-E.; Weaver, D.; Carr, S.A.; et al. DNA Damage Activates a Spatially Distinct Late Cytoplasmic Cell-Cycle Checkpoint Network Controlled by MK2-Mediated RNA Stabilization. *Mol. Cell* **2010**, *40*, 34–49, doi:10.1016/j.molcel.2010.09.018.
80. Mittal, P.; Roberts, C.W.M. The SWI/SNF Complex in Cancer - Biology, Biomarkers and Therapy. *Nat. Rev. Clin. Oncol.* **2020**, *17*, 435–448, doi:10.1038/s41571-020-0357-3.
81. Gañez-Zapater, A.; Mackowiak, S.D.; Guo, Y.; Tarbier, M.; Jordán-Pla, A.; Friedländer, M.R.; Visa, N.; Östlund Farrants, A.-K. The SWI/SNF Subunit BRG1 Affects Alternative Splicing by Changing RNA Binding Factor Interactions with Nascent RNA. *Mol. Genet. Genomics* **2022**, *297*, 463–484, doi:10.1007/s00438-022-01863-9.
82. Söderberg, O.; Gullberg, M.; Jarvius, M.; Ridderstråle, K.; Leuchowius, K.-J.; Jarvius, J.; Wester, K.; Hydbring, P.; Bahram, F.; Larsson, L.-G.; et al. Direct Observation of Individual Endogenous Protein Complexes in Situ by Proximity Ligation. *Nat. Methods* **2006**, *3*, 995–1000, doi:10.1038/nmeth947.
83. Post, G.R.; Dawson, G. Characterization of a Cell Line Derived from a Human Oligodendroglioma. *Mol. Chem. Neuropathol.* **1992**, *16*, 303–317.
84. Ahmad, S.T.; Rogers, A.D.; Chen, M.J.; Dixit, R.; Adnani, L.; Frankiw, L.S.; Lawn, S.O.; Blough, M.D.; Alshehri, M.; Wu, W.; et al. Capicua Regulates Neural Stem Cell Proliferation and Lineage Specification through Control of Ets Factors. *Nat. Commun.* **2019**, *10*, 2000, doi:10.1038/s41467-019-09949-6.
85. Cooper, S. Rethinking Synchronization of Mammalian Cells for Cell Cycle Analysis. *Cell. Mol. Life Sci.* **2003**, *60*, 1099–1106, doi:10.1007/s00018-003-2253-2.
86. Hsiao, C.J.; Tung, P.; Blischak, J.D.; Burnett, J.E.; Barr, K.A.; Dey, K.K.; Stephens, M.; Gilad, Y. Characterizing and Inferring Quantitative Cell Cycle Phase in Single-Cell RNA-Seq Data Analysis. *Genome Res.* **2020**, *30*, 611–621, doi:10.1101/gr.247759.118.
87. Whitfield, M.L.; Sherlock, G.; Saldanha, A.J.; Murray, J.I.; Ball, C.A.; Alexander, K.E.; Matese, J.C.; Perou, C.M.; Hurt, M.M.; Brown, P.O.; et al. Identification of Genes Periodically Expressed in the Human Cell Cycle and Their Expression in Tumors. *Mol. Biol. Cell* **2002**, *13*, 1977–2000, doi:10.1091/mbc.02-02-0030.
88. Macosko, E.Z.; Basu, A.; Satija, R.; Nemesh, J.; Shekhar, K.; Goldman, M.; Tirosh, I.; Bialas, A.R.; Kamitaki, N.; Martersteck, E.M.; et al. Highly Parallel Genome-Wide Expression Profiling of Individual Cells Using Nanoliter Droplets. *Cell* **2015**, *161*, 1202–1214, doi:10.1016/j.cell.2015.05.002.
89. Schwabe, D.; Formichetti, S.; Junker, J.P.; Falcke, M.; Rajewsky, N. The Transcriptome Dynamics of Single Cells during the Cell Cycle. *Mol. Syst. Biol.* **2020**, *16*, e9946, doi:10.15252/msb.20209946.
90. Conte, A.; Valente, V.; Paladino, S.; Pierantoni, G.M. HIPK2 in Cancer Biology and Therapy: Recent Findings and Future Perspectives. *Cell. Signal.* **2023**, *101*, 110491, doi:10.1016/j.cellsig.2022.110491.
91. Meister, G.; Landthaler, M.; Peters, L.; Chen, P.Y.; Urlaub, H.; Lührmann, R.; Tuschl, T. Identification of Novel Argonaute-Associated Proteins. *Curr. Biol.* **2005**, *15*, 2149–2155, doi:10.1016/j.cub.2005.10.048.
92. Lazzaretti, D.; Tournier, I.; Izaurralde, E. The C-Terminal Domains of Human TNRC6A, TNRC6B, and TNRC6C Silence Bound Transcripts Independently of Argonaute Proteins. *RNA* **2009**, *15*,

1059–1066, doi:10.1261/rna.1606309.
93. Pong, S.K.; Gullerova, M. Noncanonical Functions of microRNA Pathway Enzymes - Drosha, DGCR8, Dicer and Ago Proteins. *FEBS Lett.* **2018**, *592*, 2973–2986, doi:10.1002/1873-3468.13196.
94. Park, J.-W.; Kilic, O.; Deo, M.; Jimenez-Cowell, K.; Demirdizen, E.; Kim, H.; Turcan, Ş. CIC Reduces xCT/SLC7A11 Expression and Glutamate Release in Glioma. *Acta Neuropathol Commun* **2023**, *11*, 13, doi:10.1186/s40478-023-01507-y.
95. Dissanayake, K.; Toth, R.; Blakey, J.; Olsson, O.; Campbell, D.G.; Prescott, A.R.; MacKintosh, C. ERK/p90(RSK)/14-3-3 Signalling Has an Impact on Expression of PEA3 Ets Transcription Factors via the Transcriptional Repressor Capicua. *Biochem. J* **2011**, *433*, 515–525, doi:10.1042/BJ20101562.
96. Gardino, A.K.; Yaffe, M.B. 14-3-3 Proteins as Signaling Integration Points for Cell Cycle Control and Apoptosis. *Semin. Cell Dev. Biol.* **2011**, *22*, 688–695, doi:10.1016/j.semcdb.2011.09.008.
97. Heath, E.M.; Chan, S.M.; Minden, M.D.; Murphy, T.; Shlush, L.I.; Schimmer, A.D. Biological and Clinical Consequences of NPM1 Mutations in AML. *Leukemia* **2017**, *31*, 798–807, doi:10.1038/leu.2017.30.
98. Sobolev, V.V.; Khashukoeva, A.Z.; Evina, O.E.; Geppe, N.A.; Chebysheva, S.N.; Korsunskaya, I.M.; Tchepourina, E.; Mezentsev, A. Role of the Transcription Factor FOSL1 in Organ Development and Tumorigenesis. *Int. J. Mol. Sci.* **2022**, *23*, doi:10.3390/ijms23031521.
99. Chaudhari, H.G.; Cohen, B.A. Local Sequence Features That Influence AP-1 Cis-Regulatory Activity. *Genome Res.* **2018**, *28*, 171–181, doi:10.1101/gr.226530.117.
100. Kannan, M.B.; Solovieva, V.; Blank, V. The Small MAF Transcription Factors MAFF, MAFG and MAFK: Current Knowledge and Perspectives. *Biochim. Biophys. Acta* **2012**, *1823*, 1841–1846, doi:10.1016/j.bbamcr.2012.06.012.
101. Katsuoka, F.; Yamamoto, M. Small Maf Proteins (MafF, MafG, MafK): History, Structure and Function. *Gene* **2016**, *586*, 197–205, doi:10.1016/j.gene.2016.03.058.
102. Amit, I.; Citri, A.; Shay, T.; Lu, Y.; Katz, M.; Zhang, F.; Tarcic, G.; Siwak, D.; Lahad, J.; Jacob-Hirsch, J.; et al. A Module of Negative Feedback Regulators Defines Growth Factor Signaling. *Nat. Genet.* **2007**, *39*, 503–512, doi:10.1038/ng1987.
103. Owens, D.M.; Keyse, S.M. Differential Regulation of MAP Kinase Signalling by Dual-Specificity Protein Phosphatases. *Oncogene* **2007**, *26*, 3203–3213, doi:10.1038/sj.onc.1210412.
104. Hu, J.; Yao, H.; Gan, F.; Tokarski, A.; Wang, Y. Interaction of OKL38 and p53 in Regulating Mitochondrial Structure and Function. *PLoS One* **2012**, *7*, e43362, doi:10.1371/journal.pone.0043362.
105. Gatchalian, J.; Malik, S.; Ho, J.; Lee, D.-S.; Kelso, T.W.R.; Shokhirev, M.N.; Dixon, J.R.; Hargreaves, D.C. A Non-Canonical BRD9-Containing BAF Chromatin Remodeling Complex Regulates Naive Pluripotency in Mouse Embryonic Stem Cells. *Nat. Commun.* **2018**, *9*, 5139, doi:10.1038/s41467-018-07528-9.
106. Sterne-Weiler, T.; Weatheritt, R.J.; Best, A.J.; Ha, K.C.H.; Blencowe, B.J. Efficient and Accurate Quantitative Profiling of Alternative Splicing Patterns of Any Complexity on a Laptop. *Mol. Cell* **2018**, *72*, 187–200.e6, doi:10.1016/j.molcel.2018.08.018.
107. Melé, M.; Ferreira, P.G.; Reverter, F.; DeLuca, D.S.; Monlong, J.; Sammeth, M.; Young, T.R.; Goldmann, J.M.; Pervouchine, D.D.; Sullivan, T.J.; et al. Human Genomics. The Human Transcriptome across Tissues and Individuals. *Science* **2015**, *348*, 660–665, doi:10.1126/science.aaa0355.
108. Georgakopoulos-Soares, I.; Parada, G.E.; Wong, H.Y.; Medhi, R.; Furlan, G.; Munita, R.; Miska, E.A.; Kwok, C.K.; Hemberg, M. Alternative Splicing Modulation by G-Quadruplexes. *Nat. Commun.* **2022**, *13*, 2404, doi:10.1038/s41467-022-30071-7.
109. Kolas, N.K.; Chapman, J.R.; Nakada, S.; Ylanko, J.; Chahwan, R.; Sweeney, F.D.; Panier, S.; Mendez, M.; Wildenhain, J.; Thomson, T.M.; et al. Orchestration of the DNA-Damage Response by

the RNF8 Ubiquitin Ligase. *Science* **2007**, *318*, 1637–1640, doi:10.1126/science.1150034.
110. Hughes, R.; Gilley, J.; Kristiansen, M.; Ham, J. The MEK-ERK Pathway Negatively Regulates Bim Expression through the 3' UTR in Sympathetic Neurons. *BMC Neurosci.* **2011**, *12*, 69, doi:10.1186/1471-2202-12-69.
111. Moore, M.J. From Birth to Death: The Complex Lives of Eukaryotic mRNAs. *Science* **2005**, *309*, 1514–1518, doi:10.1126/science.1111443.
112. Sandberg, R.; Neilson, J.R.; Sarma, A.; Sharp, P.A.; Burge, C.B. Proliferating Cells Express mRNAs with Shortened 3' Untranslated Regions and Fewer microRNA Target Sites. *Science* **2008**, *320*, 1643–1647, doi:10.1126/science.1155390.
113. Cenik, C.; Derti, A.; Mellor, J.C.; Berriz, G.F.; Roth, F.P. Genome-Wide Functional Analysis of Human 5' Untranslated Region Introns. *Genome Biol.* **2010**, *11*, R29, doi:10.1186/gb-2010-11-3-r29.
114. Grabski, D.F.; Broseus, L.; Kumari, B.; Rekosh, D.; Hammarskjold, M.-L.; Ritchie, W. Intron Retention and Its Impact on Gene Expression and Protein Diversity: A Review and a Practical Guide. *Wiley Interdiscip. Rev. RNA* **2021**, *12*, e1631, doi:10.1002/wrna.1631.
115. Li, N.; Fassl, A.; Chick, J.; Inuzuka, H.; Li, X.; Mansour, M.R.; Liu, L.; Wang, H.; King, B.; Shaik, S.; et al. Cyclin C Is a Haploinsufficient Tumour Suppressor. *Nat. Cell Biol.* **2014**, *16*, 1080–1091, doi:10.1038/ncb3046.
116. Chen, Q.; Fu, Q.; Pu, L.; Liu, X.; Liu, Y. Effects of HMGA2 Gene Silencing on Cell Cycle and Apoptosis in the Metastatic Renal Carcinoma Cell Line ACHN. *J. Int. Med. Res.* **2022**, *50*, 3000605221075511, doi:10.1177/03000605221075511.
117. Wang, H.-X.; Qin, X.-H.; Shen, J.; Liu, Q.-H.; Shi, Y.-B.; Xue, L. Proteomic Analysis Reveals That Placenta-Specific Protein 9 Inhibits Proliferation and Stimulates Motility of Human Bronchial Epithelial Cells. *Front. Oncol.* **2021**, *11*, 628480, doi:10.3389/fonc.2021.628480.
118. Fernandez-Cuesta, L.; Thomas, R.K. Molecular Pathways: Targeting NRG1 Fusions in Lung Cancer. *Clin. Cancer Res.* **2015**, *21*, 1989–1994, doi:10.1158/1078-0432.CCR-14-0854.
119. Mei, L.; Xiong, W.-C. Neuregulin 1 in Neural Development, Synaptic Plasticity and Schizophrenia. *Nat. Rev. Neurosci.* **2008**, *9*, 437–452, doi:10.1038/nrn2392.
120. Mei, L.; Nave, K.-A. Neuregulin-ERBB Signaling in the Nervous System and Neuropsychiatric Diseases. *Neuron* **2014**, *83*, 27–49, doi:10.1016/j.neuron.2014.06.007.
121. Innis, S.M.; Cabot, B. GBAF, a Small BAF Sub-Complex with Big Implications: A Systematic Review. *Epigenetics Chromatin* **2020**, *13*, 48, doi:10.1186/s13072-020-00370-8.
122. Xue, Y.; Canman, J.C.; Lee, C.S.; Nie, Z.; Yang, D.; Moreno, G.T.; Young, M.K.; Salmon, E.D.; Wang, W. The Human SWI/SNF-B Chromatin-Remodeling Complex Is Related to Yeast Rsc and Localizes at Kinetochores of Mitotic Chromosomes. *Proc. Natl. Acad. Sci. U. S. A.* **2000**, *97*, 13015–13020, doi:10.1073/pnas.240208597.
123. Rahman, S.; Sowa, M.E.; Ottinger, M.; Smith, J.A.; Shi, Y.; Harper, J.W.; Howley, P.M. The Brd4 Extraterminal Domain Confers Transcription Activation Independent of pTEFb by Recruiting Multiple Proteins, Including NSD3. *Mol. Cell. Biol.* **2011**, *31*, 2641–2652, doi:10.1128/MCB.01341-10.
124. Coisy-Quivy, M.; Disson, O.; Roure, V.; Muchardt, C.; Blanchard, J.-M.; Dantonel, J.-C. Role for Brm in Cell Growth Control. *Cancer Res.* **2006**, *66*, 5069–5076, doi:10.1158/0008-5472.CAN-05-0596.
125. Dykhuizen, E.C.; Hargreaves, D.C.; Miller, E.L.; Cui, K.; Korshunov, A.; Kool, M.; Pfister, S.; Cho, Y.J.; Zhao, K.; Crabtree, G.R. BAF Complexes Facilitate Decatenation of DNA by Topoisomerase IIalpha. *Nature* **2013**, *497*, 624–627, doi:10.1038/nature12146.
126. Brownlee, P.M.; Chambers, A.L.; Cloney, R.; Bianchi, A.; Downs, J.A. BAF180 Promotes Cohesion and Prevents Genome Instability and Aneuploidy. *Cell Rep.* **2014**, *6*, 973–981, doi:10.1016/j.celrep.2014.02.012.
127. You, S.Y.; Park, Y.S.; Jeon, H.-J.; Cho, D.-H.; Jeon, H.B.; Kim, S.H.; Chang, J.W.; Kim, J.-S.;

Oh, J.S. Beclin-1 Knockdown Shows Abscission Failure but Not Autophagy Defect during Oocyte Meiotic Maturation. *Cell Cycle* **2016**, *15*, 1611–1619, doi:10.1080/15384101.2016.1181235.
128. Ricke, R.M.; Jeganathan, K.B.; van Deursen, J.M. Bub1 Overexpression Induces Aneuploidy and Tumor Formation through Aurora B Kinase Hyperactivation. *J. Cell Biol.* **2011**, *193*, 1049–1064, doi:10.1083/jcb.201012035.
129. Zhang, T.; Zhou, Y.; Qi, S.-T.; Wang, Z.-B.; Qian, W.-P.; Ouyang, Y.-C.; Shen, W.; Schatten, H.; Sun, Q.-Y. Nuf2 Is Required for Chromosome Segregation during Mouse Oocyte Meiotic Maturation. *Cell Cycle* **2015**, *14*, 2701–2710, doi:10.1080/15384101.2015.1058677.
130. Holmes, Z.E.; Hamilton, D.J.; Hwang, T.; Parsonnet, N.V.; Rinn, J.L.; Wuttke, D.S.; Batey, R.T. The Sox2 Transcription Factor Binds RNA. *Nat. Commun.* **2020**, *11*, 1805, doi:10.1038/s41467-020-15571-8.
131. Lee, C.J.; Chan, W.I.; Cheung, M.; Cheng, Y.C.; Appleby, V.J.; Orme, A.T.; Scotting, P.J. CIC, a Member of a Novel Subfamily of the HMG-Box Superfamily, Is Transiently Expressed in Developing Granule Neurons. *Brain Res. Mol. Brain Res.* **2002**, *106*, 151–156.
132. Somma, M.P.; Andreyeva, E.N.; Pavlova, G.A.; Pellacani, C.; Bucciarelli, E.; Popova, J.V.; Bonaccorsi, S.; Pindyurin, A.V.; Gatti, M. Moonlighting in Mitosis: Analysis of the Mitotic Functions of Transcription and Splicing Factors. *Cells* **2020**, *9*, doi:10.3390/cells9061554.
133. Ajuh, P.; Kuster, B.; Panov, K.; Zomerdijk, J.C.; Mann, M.; Lamond, A.I. Functional Analysis of the Human CDC5L Complex and Identification of Its Components by Mass Spectrometry. *EMBO J.* **2000**, *19*, 6569–6581, doi:10.1093/emboj/19.23.6569.
134. Mu, R.; Wang, Y.-B.; Wu, M.; Yang, Y.; Song, W.; Li, T.; Zhang, W.-N.; Tan, B.; Li, A.-L.; Wang, N.; et al. Depletion of Pre-mRNA Splicing Factor Cdc5L Inhibits Mitotic Progression and Triggers Mitotic Catastrophe. *Cell Death Dis.* **2014**, *5*, e1151, doi:10.1038/cddis.2014.117.
135. Munschauer, M.; Nguyen, C.T.; Sirokman, K.; Hartigan, C.R.; Hogstrom, L.; Engreitz, J.M.; Ulirsch, J.C.; Fulco, C.P.; Subramanian, V.; Chen, J.; et al. The NORAD lncRNA Assembles a Topoisomerase Complex Critical for Genome Stability. *Nature* **2018**, *561*, 132–136, doi:10.1038/s41586-018-0453-z.
136. Weg-Remers, S.; Ponta, H.; Herrlich, P.; König, H. Regulation of Alternative Pre-mRNA Splicing by the ERK MAP-Kinase Pathway. *EMBO J.* **2001**, *20*, 4194–4203, doi:10.1093/emboj/20.15.4194.
137. Wei, C.; Peng, B.; Han, Y.; Chen, W.V.; Rother, J.; Tomlinson, G.E.; Boland, C.R.; Chaussabel, D.; Frazier, M.L.; Amos, C.I. Mutations of HNRNPA0 and WIF1 Predispose Members of a Large Family to Multiple Cancers. *Fam. Cancer* **2015**, *14*, 297–306, doi:10.1007/s10689-014-9758-8.
138. R Core Team *R: A Language and Environment for Statistical Computing*; R Foundation for Statistical Computing: Vienna, Austria, 2020;.
139. Lun, A.T.; Bach, K.; Marioni, J.C. Pooling across Cells to Normalize Single-Cell RNA Sequencing Data with Many Zero Counts. *Genome Biol.* **2016**, *17*, 75, doi:10.1186/s13059-016-0947-7.
140. Zheng, S.C.; Stein-O'Brien, G.; Augustin, J.J.; Slosberg, J.; Carosso, G.A.; Winer, B.; Shin, G.; Bjornsson, H.T.; Goff, L.A.; Hansen, K.D. Universal Prediction of Cell-Cycle Position Using Transfer Learning. *Genome Biol.* **2022**, *23*, 41, doi:10.1186/s13059-021-02581-y.
141. Love, M.I.; Huber, W.; Anders, S. Moderated Estimation of Fold Change and Dispersion for RNA-Seq Data with DESeq2. *Genome Biol.* **2014**, *15*, 550, doi:10.1186/s13059-014-0550-8.
142. Takemon, Y.; Marra, M.A. GRETA: An R Package for Mapping in Silico Genetic Interaction and Essentiality Networks. *bioRxiv* 2022, 2022.09.21.508787.
143. Pan, J.; Meyers, R.M.; Michel, B.C.; Mashtalir, N.; Sizemore, A.E.; Wells, J.N.; Cassel, S.H.; Vazquez, F.; Weir, B.A.; Hahn, W.C.; et al. Interrogation of Mammalian Protein Complex Structure, Function, and Membership Using Genome-Scale Fitness Screens. *Cell Syst* **2018**, *6*, 555–568.e7, doi:10.1016/j.cels.2018.04.011.

144. Li, H.; Durbin, R. Fast and Accurate Short Read Alignment with Burrows-Wheeler Transform. *Bioinformatics* **2009**, *25*, 1754–1760, doi:10.1093/bioinformatics/btp324.
145. Li, H.; Handsaker, B.; Wysoker, A.; Fennell, T.; Ruan, J.; Homer, N.; Marth, G.; Abecasis, G.; Durbin, R.; 1000 Genome Project Data Processing Subgroup The Sequence Alignment/Map Format and SAMtools. *Bioinformatics* **2009**, *25*, 2078–2079, doi:10.1093/bioinformatics/btp352.
146. Danecek, P.; Bonfield, J.K.; Liddle, J.; Marshall, J.; Ohan, V.; Pollard, M.O.; Whitwham, A.; Keane, T.; McCarthy, S.A.; Davies, R.M.; et al. Twelve Years of SAMtools and BCFtools. *Gigascience* **2021**, *10*, doi:10.1093/gigascience/giab008.
147. Zhang, Y.; Liu, T.; Meyer, C.A.; Eeckhoute, J.; Johnson, D.S.; Bernstein, B.E.; Nusbaum, C.; Myers, R.M.; Brown, M.; Li, W.; et al. Model-Based Analysis of ChIP-Seq (MACS). *Genome Biol.* **2008**, *9*, R137, doi:10.1186/gb-2008-9-9-r137.
148. Yu, G.; Wang, L.-G.; He, Q.-Y. ChIPseeker: An R/Bioconductor Package for ChIP Peak Annotation, Comparison and Visualization. *Bioinformatics* **2015**, *31*, 2382–2383, doi:10.1093/bioinformatics/btv145.
149. Wang, Q.; Li, M.; Wu, T.; Zhan, L.; Li, L.; Chen, M.; Xie, W.; Xie, Z.; Hu, E.; Xu, S.; et al. Exploring Epigenomic Datasets by ChIPseeker. *Curr Protoc* **2022**, *2*, e585, doi:10.1002/cpz1.585.
150. Lawrence, M.; Huber, W.; Pages, H.; Aboyoun, P.; Carlson, M.; Gentleman, R.; Morgan, M.T.; Carey, V.J. Software for Computing and Annotating Genomic Ranges. *PLoS Comput. Biol.* **2013**, *9*, e1003118, doi:10.1371/journal.pcbi.1003118.
151. Zhu, L.J.; Gazin, C.; Lawson, N.D.; Pagès, H.; Lin, S.M.; Lapointe, D.S.; Green, M.R. ChIPpeakAnno: A Bioconductor Package to Annotate ChIP-Seq and ChIP-Chip Data. *BMC Bioinformatics* **2010**, *11*, 237, doi:10.1186/1471-2105-11-237.
152. Zhu, L.J. Integrative Analysis of ChIP-Chip and ChIP-Seq Dataset. In *Tiling Arrays: Methods and Protocols*; Lee, T.-L., Shui Luk, A.C., Eds.; Humana Press: Totowa, NJ, 2013; pp. 105–124 ISBN 9781627036078.
153. Thorvaldsdóttir, H.; Robinson, J.T.; Mesirov, J.P. Integrative Genomics Viewer (IGV): High-Performance Genomics Data Visualization and Exploration. *Brief. Bioinform.* **2013**, *14*, 178–192, doi:10.1093/bib/bbs017.
154. Perez-Riverol, Y.; Csordas, A.; Bai, J.; Bernal-Llinares, M.; Hewapathirana, S.; Kundu, D.J.; Inuganti, A.; Griss, J.; Mayer, G.; Eisenacher, M.; et al. The PRIDE Database and Related Tools and Resources in 2019: Improving Support for Quantification Data. *Nucleic Acids Res.* **2019**, *47*, D442–D450, doi:10.1093/nar/gky1106.
155. Perkins, D.N.; Pappin, D.J.; Creasy, D.M.; Cottrell, J.S. Probability-Based Protein Identification by Searching Sequence Databases Using Mass Spectrometry Data. *Electrophoresis* **1999**, *20*, 3551–3567, doi:10.1002/(SICI)1522-2683(19991201)20:18<3551::AID-ELPS3551>3.0.CO;2-2.
156. UniProt Consortium UniProt: The Universal Protein Knowledgebase in 2021. *Nucleic Acids Res.* **2021**, *49*, D480–D489, doi:10.1093/nar/gkaa1100.
157. Bairoch, A.; Apweiler, R. The SWISS-PROT Protein Sequence Database and Its Supplement TrEMBL in 2000. *Nucleic Acids Res.* **2000**, *28*, 45–48, doi:10.1093/nar/28.1.45.
158. Hughes, C.S.; Foehr, S.; Garfield, D.A.; Furlong, E.E.; Steinmetz, L.M.; Krijgsveld, J. Ultrasensitive Proteome Analysis Using Paramagnetic Bead Technology. *Mol. Syst. Biol.* **2014**, *10*, 757, doi:10.15252/msb.20145625.
159. Hughes, C.S.; McConechy, M.K.; Cochrane, D.R.; Nazeran, T.; Karnezis, A.N.; Huntsman, D.G.; Morin, G.B. Quantitative Profiling of Single Formalin Fixed Tumour Sections: Proteomics for Translational Research. *Scientific Reports* 2016, *6*.
160. Zolg, D.P.; Wilhelm, M.; Schnatbaum, K.; Zerweck, J.; Knaute, T.; Delanghe, B.; Bailey, D.J.; Gessulat, S.; Ehrlich, H.-C.; Weininger, M.; et al. Building ProteomeTools Based on a Complete Synthetic Human Proteome. *Nature Methods* 2017, *14*, 259–262.
161. Rappsilber, J.; Ishihama, Y.; Mann, M. Stop and Go Extraction Tips for Matrix-Assisted Laser

Desorption/Ionization, Nanoelectrospray, and LC/MS Sample Pretreatment in Proteomics. *Analytical Chemistry* 2003, *75*, 663–670.
162. Käll, L.; Canterbury, J.D.; Weston, J.; Noble, W.S.; MacCoss, M.J. Semi-Supervised Learning for Peptide Identification from Shotgun Proteomics Datasets. *Nature Methods* 2007, *4*, 923–925.
163. Spivak, M.; Weston, J.; Bottou, L.; Käll, L.; Noble, W.S. Improvements to the Percolator Algorithm for Peptide Identification from Shotgun Proteomics Data Sets. *Journal of Proteome Research* 2009, *8*, 3737–3745.